Science

RESEARCH ARTICLES

Cite as: J. Qian *et al.*, *Science* 10.1126/science.adv0134 (2025).

# Chromatin buffers torsional stress during transcription

**Jin Qian[1,2], Lucyna Lubkowska[3], Shuming Zhang[1,2], Chuang Tan[1,2], Yifeng Hong[4], Xiaomeng Jia[1,2], Robert M. Fulbright[1], James T. Inman[1,2], Taryn M. Kay[5], Joshua Jeong[6], Glenn Hauk[6], Deanna Gotte[7], James M. Berger[6], Mikhail Kashlev[3], Michelle D. Wang[1,2]***

[1]Department of Physics and LASSP, Cornell University, Ithaca, NY, USA. [2]Howard Hughes Medical Institute, Cornell University, Ithaca, NY, USA. [3]RNA Biology Laboratory, Center for Cancer Research, National Cancer Institute, Frederick, MD, USA. [4]Department of Electrical and Computer Engineering, Cornell University, Ithaca, NY, USA. [5]Biophysics Program, Cornell University, Ithaca, NY, USA. [6]Department of Biophysics and Biophysical Chemistry, Johns Hopkins University School of Medicine, Baltimore, MD, USA. [7]HIV Dynamics and Replication Program, Center for Cancer Research, National Cancer Institute, Frederick, MD, USA.

***Corresponding author. Email: mwang@physics.cornell.edu**

**During eukaryotic transcription, Pol II must overcome nucleosome obstacles and, because of DNA's helical structure, must also rotate relative to DNA, generating torsional stress. However, there is limited understanding of how Pol II transcribes through nucleosomes while supercoiling DNA. Here, we determined that Pol II generates a torque of 9 pN·nm alone and 13 pN·nm with TFIIS, making it a powerful rotary motor. When Pol II encounters a nucleosome, passage becomes more efficient on a chromatin substrate than on a single-nucleosome substrate, demonstrating that chromatin significantly buffers torsional stress during transcription. Furthermore, topoisomerase supercoiling relaxation allows Pol II to transcribe through multiple nucleosomes. Our results reveal a role of chromatin beyond the more conventional view of it being just a roadblock to transcription.**



Because of the DNA helical nature, during transcription elongation, RNA polymerase (RNAP) and DNA must rotate relative to each other as RNAP translocates along the DNA. In vivo, RNAP rotation is thought to be restricted due to the viscous drag of large molecular machineries, such as spliceosomes, associated with the nascent RNA (*1*), thus, the DNA at the RNAP must rotate. This obligatory relative rotation, dictated by the helical nature of DNA (*2*, *3*), imposes one turn for every 10.5 nt transcribed by RNAP. Consequently, RNAP tightly couples its translocation and rotation, making it concurrently a linear motor to generate force to translocate and a rotary motor to generate torque to rotate (*4*, *5*). This torque measures the torsional stress that RNAP experiences while supercoiling DNA. These inherent motor properties are crucial for gene expression, enabling RNAP to overcome roadblocks and reconfigure DNA structures and topology (*6*, *7*). Notably, the rotational motion leads to DNA supercoiling and torsional stress in the DNA, which, in turn, regulates transcription (*6*–*14*). It is important to note that while supercoiling refers to extra turns introduced into DNA, torque measures how difficult it is to introduce those turns, reflecting RNAP's capacity to rotate the DNA while working against the resistance. Yet our understanding of how RNAP generates torque and works against torsional stress is limited. Previously, we found that *E. coli* RNAP is a powerful rotary motor capable of generating sufficient torque to melt DNA (*13*, *14*). Whether the eukaryotic RNA polymerase II (Pol II) can do the same remains unknown.

Recent studies have highlighted the diverse critical roles of transcription-generated DNA torsional stress in cellular functions (*15*–*18*). Torsional stress on DNA is present across the genome and regulates gene expression, even in the presence of native topoisomerases (*15*, *19*–*26*). The torsional stress generated from the transcription of one gene can also regulate the expression of other genes in the vicinity (*7*, *10*, *27*, *28*). Moreover, DNA torsion accumulation during a head-on conflict of transcription and replication has been suggested to promote persistent replication stress and subsequent DNA damage (*29*–*31*). It is worth noting that because torsional stress in DNA can act over a distance, this consequence may occur well before any physical encounter of RNAP with the replisome (*29*, *32*). Furthermore, transcription-generated torsional stress has also been found to significantly change DNA topology by regulating 3D genome knotting, folding, loop formation, and DNA structures (*33*, *34*).

Eukaryotic RNAP Pol II must transcribe through nucleosomes; thus, transcription through chromatin under torsion represents a fundamental problem in biology. Despite the significance of this problem, little is known about how Pol II transcribes through chromatin while supercoiling DNA. Chromatin is commonly perceived as a roadblock to transcription elongation, but this perception must be revisited, especially in the context of transcription under torsion. Notably, while DNA assumes a right-handed helical structure, each nucleosome in chromatin has DNA wrapping around the core histones in a left-handed fashion (*35*). However, it is unclear how DNA chirality and nucleosome chirality work together to impact Pol II's ability to transcribe through nucleosomes. The complexity of this problem poses significant challenges to experimental investigation and requires new methodologies and conceptualizations to gain mechanistic understanding. Previous structural, biochemical, and single-

molecule studies focused on transcription through a single-nucleosome without consideration of transcription-generated torsional stress. In this work, we have enabled this investigation by developing several highly sophisticated single-molecule methods. Our study has uncovered significant and quantitative insights into a role of chromatin during transcription under torsion.

**Visualizing Pol II rotation of DNA**

The fundamental cause of transcription-generated torsional stress is RNAP rotation of torsionally constrained DNA. Understanding this rotation requires a real-time method for visualizing the rotational motion when transcription occurs at a specified torsional stress level. Previously, the rotational motion for *E. coli* RNAP was detected/inferred via the rotation of a bead (*36*), the rotation of a DNA origami attached to the DNA (*37*), or RNAP-generated DNA supercoiling (*13*, *14*). However, these methods either do not allow on-demand control of the torsional stress or do not directly track the rotation.

Here, we present an approach to directly track Pol II-generated rotation of DNA at high spatial and temporal resolution using an angular optical trap (AOT). A defining feature of the AOT is its trapping particle, a nanofabricated birefringent quartz cylinder (Fig. 1A and fig. S1), which serves as a handle for simultaneous measurements of force, extension, torque, and rotation of DNA (*38–42*). The angular orientation of the quartz cylinder can be detected at an exceedingly high angular and temporal resolution (*43–45*) and thus can be used to visualize how Pol II induces DNA rotation.

To apply the AOT to Pol II, we torsionally constrained *S. cerevisiae* Pol II (fig. S2) to the coverslip surface of a sample chamber and its downstream DNA to the bottom of the cylinder (Fig. 1A, figs. S3 and S4, and tables S1 and S2). Pol II translocation leads to positive (+) torque buildup, which ultimately buckles the DNA to form a plectoneme (fig. S5). Once the torque reached a desired value, the AOT rotates the cylinder to follow Pol II rotation of DNA, thus limiting further torque buildup and maintaining a constant torque. At this point, for each turn of Pol II rotation of the DNA (10.5 bp transcribed), the cylinder also rotates by a turn (Materials and methods). Because the cylinder's extraordinary axis angle can be tracked at exceedingly high spatial and temporal resolution (*43–45*), this method provides unprecedented resolution of the Pol II rotational motion.

The example trace in Fig. 1B shows Pol II rotation of DNA under 3.2 pN·nm resisting torque. This torque is relatively low compared with the magnitude of the torque required to melt DNA (*40*), mimicking an in vivo condition where topoisomerases can almost keep up with transcription. As Pol II progresses along the DNA, it exhibits steady rotational motion (1-2 turns/s), interspersed by pauses. This rotational motion, also visualized in movie S1, corresponds to an overall rate of 10-20 nt/s elongation rate, comparable to those determined when RNAP rotation was not topologically constrained in previous in vitro experiments (*46–52*). This indicates that a torque of 3.2 pN·nm does not substantially slow down Pol II elongation. These Pol II rotational behaviors are also reminiscent of the translocational motions of RNAP from previous studies (*46–49*, *51*, *52*), reflecting the translocation-rotation coupling of RNAP. The direct visualization of the Pol II rotational motion highlights the inherent nature of rotational motion during transcription and invites the investigation of the inevitable consequences of transcription-generated rotation.

**Pol II is a powerful rotary motor**

In vivo, Pol II-generated DNA supercoiling cannot be fully dissipated by rotation of the DNA ends, which are often associated with cellular structures, domains, or factories (*1*). Consequently, transcription accumulates positive (+) supercoiling and torsional stress in front of Pol II and negative (−) supercoiling and torsional stress behind, leading to the well-known "twin-supercoiled-domain" model of transcription (*26*, *53*). Both the (+) torsional stress in front of Pol II and the (−) torsional stress behind it hinder transcription. These torsional buildups can occur even in the presence of topoisomerases (*15*, *19–26*), suggesting that topoisomerases cannot always keep up with transcription. Especially when there is a transient shortage of topoisomerases near an active gene, torsional stress in the DNA can build up, leading to Pol II stalling. The torque at which Pol II stalls determines Pol II's torsional capacity to work against torsional stress and modulate the DNA topology. However, it is unknown how much torque Pol II can generate before stalling.

To measure Pol II's stall torque, we adapted a method we previously used for stall torque measurements of *E. coli* RNAP using an AOT (*13*, *14*). Instead of rotating the cylinder as in Fig. 1A, we restricted the cylinder rotation, allowing Pol II to build up torsional stress on the DNA and eventually stall (Fig. 1C). During this process, we monitored how Pol II moves along the DNA and generates torsional stress in real-time (Fig. 1D). We investigated two stalling configurations: Pol II accumulation of (−) supercoiling behind or (+) supercoiling in the front and found that the stall torque magnitudes are similar in these two configurations despite being opposite in rotational sense: −9.0 ± 1.4 pN·nm (mean ± SD) and +8.5 ± 1.9 pN·nm, respectively. For comparison, the DNA melting torque is around −10 pN·nm (*40*), suggesting that Pol II is a torsional motor almost sufficiently powerful to melt DNA.

**TFIIS enhances Pol II's torsional capacity**

Upon stalling under torsion, we observed that Pol II often

reverses its movement and moves backward by up to 100 bp or more while relaxing the transcription-generated torsional stress (Fig. 1D and fig. S6). This reverse motion is consistent with Pol II backtracking, during which Pol II reversely translocates along DNA, threading its 3′ transcribed RNA through the secondary channel and rendering Pol II inactive (*54*–*57*). This observation shows that backtracking is the primary cause for stalling under torsion, indicating that anti-backtracking transcription elongation factors, such as TFIIS (*54*, *58*–*60*), may facilitate Pol II transcription under torsion by stimulating the cleavage activity of Pol II and rescuing the backtracked complexes in a way similar to the effect of GreB on *E. coli* RNAP (*14*).

Investigating whether TFIIS can facilitate Pol II transcription under torsion and, more broadly, how Pol II works against obstacles requires extensive exploration of broad experimental conditions, which is challenging when measurements must be conducted sequentially on the AOT. The scope of this investigation motivated us to develop an alternative method using magnetic tweezers (MT), which enable parallel measurements of multiple molecules while resolving the dynamics of each molecule (*11*, *12*, *34*, *61*–*64*). Although the MT instrument cannot directly measure torque, the torque on the DNA substrate may be obtained through the measured DNA extension and force using the DNA torsional properties established from the AOT (fig. S5 and table S2).

We first used the MT assay to determine the stall torque of Pol II in the presence of TFIIS. In this experiment, we anchored Pol II to a magnetic bead and torsionally constrained the downstream DNA to the coverslip surface of a sample chamber (Fig. 2A). Previously, we showed that *E. coli* RNAP stall torque may be obtained via a torque-jump method using the AOT (*13*). We adapted this method for Pol II stall torque measurements on the MT. We first verified that Pol II was active under an assisting torque by allowing it to transcribe under (−) supercoiling (Materials and methods). Continued transcription converts the (−) supercoiling to (+) supercoiling and buckles the DNA to form a (+) buckled plectoneme at +6 pN·nm torque. We then jumped the torque to a higher value, for example, +10 pN·nm (Fig. 2B), and determined whether Pol II could continue moving forward (Materials and methods). In the example trace without TFIIS (Fig. 2B), Pol II stalls and extensively backtracks, with the backtracking distance increasing with time, indicating +10 pN·nm is substantial resistance to forward movement. In contrast, in the presence of TFIIS (Fig. 2B), Pol II still backtracks. However, after backtracking, Pol II resumes forward translocation, consistent with TFIIS rescuing the backtracked elongation complex. Thus, Pol II continues to move forward despite the +10 pN·nm resistant torque.

In vivo, the torsional stress in DNA is regulated by topoisomerase activity: high torsional stress when topoisomerase activity is low, and low torsional stress when topoisomerase activity is high. Our torque-jump experiment mimics this process by examining Pol II activity at different torques. Figure 2C shows the mean trajectories of Pol II. Under low torque values (such as 0 and +6 pN·nm), Pol II moves forward steadily, showing minimal differences with and without TFIIS. However, when the torque increases to +10 pN·nm, Pol II without TFIIS cannot sustain steady forward movement and backtracks extensively; in contrast, Pol II with TFIIS can still move forward. We examined the pause-free velocity, which reflects primarily the behavior of transcription elongation along the main reaction pathway (*65*, *66*). The resulting torque-velocity relation, akin to the force-velocity relation and characteristic of the chemo-mechanical property of a motor protein (*13*, *66*), shows that Pol II pause-free velocity decreases with an increase in the resisting torque (Fig. 2D). Although TFIIS substantially increases the overall ability of Pol II to move forward against torsional stress (Fig. 2C), TFIIS does not increase the pause-free velocity (Fig. 2D), consistent with TFIIS acting only on the backtracked elongation complex of the branched pathway. The measured torque-velocity relation shows a good agreement with that expected of *E. coli* RNAP (*65*, *66*) (fig. S7), suggesting that Pol II may have energetic and kinetic properties in the main reaction pathway similar to those of *E. coli* RNAP.

To determine the stall torque of Pol II, we measured the fraction of Pol II molecules remaining active at different torques (Fig. 2E). We define stall torque as the torque when 50% of the molecules remain active (*13*). This analysis shows that Pol II alone can generate +8.6 ± 0.3 pN·nm torque, consistent with values measured using the AOT within the measurement uncertainty. The presence of TFIIS increases Pol II stall torque to +12.8 ± 0.4 pN·nm, representing a 49% enhancement. Thus, TFIIS enables Pol II to work more effectively against torsional stress.

As a comparison, *E. coli* RNAP alone generates ~ +11 pN·nm torque (*13*). So, Pol II generates a torque comparable to *E. coli* RNAP, though slightly smaller. In addition, *E. coli* RNAP's torsional generation capacity is also enhanced by the anti-backtracking factor GreB to +18.5 pN·nm torque (*14*). Thus, the torsional capacity enhancement by anti-backtracking transcription elongation factors may be general to all transcription machineries. These factors may rescue backtracked complexes, and subsequent resumption of transcription provides a renewed opportunity for RNAP to work against a greater torque (*14*). Overall, the basal machinery of eukaryotic transcription is a powerful rotary motor whose torsional capacity can be regulated by transcription factors. In vivo, many other factors may potentially modulate the torsional capacity of Pol II to facilitate its passage through obstacles such as nucleosomes (*67*).

## Transcription through a nucleosome under torsion

In recent decades, through extensive in vitro and structural studies, we have gained significant mechanistic insights into the nature of the nucleosome barrier to transcription (*54*, *68*–*74*). These studies have focused primarily on transcription through a single nucleosome under no torsional stress. In the cell, Pol II must transcribe through nucleosomes in chromatin while supercoiling DNA. Thus, Pol II simultaneously experiences a physical blockage from the encountered nucleosome and resistance from supercoiling buildup in the chromatin. How chromatin impacts the ability of Pol II to transcribe through nucleosomes under torsion has remained obscure due to the complexity of this problem and a lack of experimental approaches for investigation.

To tackle this problem, we developed a real-time, magnetic tweezers-based assay to track the progression of Pol II as it transcribes through nucleosomes in a chromatin fiber (Fig. 3, A and B). The experimental configuration is similar to that of Fig. 2A, except that the downstream substrate contains either a single nucleosome or a chromatin fiber containing about 50 nucleosomes. To facilitate the comparison, the nucleosome-array template is identical to the single-nucleosome template in the number of base pairs, the transcription start site (TSS) location, and the sequence leading to and through the first nucleosome. Control experiments show that nucleosomes remain stable when subjected to a torque comparable to that Pol II might generate during transcription on a nucleosome on these templates (fig. S8).

Prior to measurements, the measured DNA extension is substantially smaller for the nucleosome-array template due to the nucleosome compaction of DNA as expected (*61*, *62*, *75*, *76*) (Fig. 3C). Upon introducing NTPs to the sample chamber, the magnetic tweezers are used to rapidly unwind each tether by 18 turns to (−) supercoil the DNA, facilitating Pol II's escape into active elongation. Subsequent transcription converts the (−) supercoiling to (+) supercoiling. With continued transcription, Pol II introduces more (+) supercoils to DNA and eventually encounters a nucleosome. We use the real-time DNA extension to monitor Pol II position along the DNA during this process (fig. S9 and Materials and methods).

In the representative traces (Fig. 3C), since Pol II position is indicated by its active site on the DNA template, the front edge of Pol II that encounters the nucleosome is about 20 bp downstream of the active site (*77*). We found that Pol II pauses when encountering the first nucleosome at about 403 bp from the TSS on the single-nucleosome template or the nucleosome-array template. The presence of TFIIS increases the ability of Pol II to move through the first nucleosome on either template. We examined the dwell time of Pol II when encountering a nucleosome in the presence of TFIIS (Fig. 3D). On the single-nucleosome template, Pol II pauses strongly before reaching the dyad of the nucleosome, with a pausing pattern indicative of periodicity (Fig. 3D, left panel). Fourier transformation of this signal reveals an ~ 11-bp periodicity (fig. S10), consistent with Pol II pausing at the strong histone-DNA interactions in a nucleosome, which occur whenever the DNA minor groove faces the histone core octamer surface (*35*, *78*). This exceptional resolution results from the detection resolution enhancement of buckled DNA: each 10.5 bp of Pol II movement leads to a ~ 5.0 nm reduction to the DNA extension. The nucleosome-array template does not allow this resolution enhancement because the extension is about ten times less sensitive to Pol II movement (fig. S11). Nonetheless, Pol II dwelling around the dyad is still detected (Fig. 3D, right panel). For both templates, the pausing patterns bear resemblance to those of transcription through a nucleosome previously observed in vitro (*70*, *79*, *80*) or through nucleosomes in the gene body in vivo (*81*–*83*), with pausing occurring primarily before and around the dyad. These observations demonstrate that we have established a method to investigate how Pol II transcribes through nucleosomes under torsion.

## Chromatin buffers torsional stress to facilitate transcription

The representative traces in Fig. 3C are suggestive that Pol II transcribes through a nucleosome more efficiently on the chromatin template than on the single-nucleosome template. To rigorously evaluate this observation, we pooled many traces and plotted the mean Pol II trajectory at their nucleosome encounter (Fig. 4A, fig. S12, and Materials and methods). Indeed, Pol II transcription is more efficient on the chromatin template. In the absence of TFIIS, Pol II stalls extensively when it first encounters the nucleosome on the single-nucleosome template. In contrast, Pol II can invade the nucleosome on the chromatin template. The presence of TFIIS greatly facilitates Pol II passage through a nucleosome on both templates, but transcription remains more efficient on the chromatin template.

Notably, for both templates, which are identical in length, Pol II transcribes the same DNA sequence and generates the same number of supercoils when encountering the nucleosome (Fig. 3A). Yet, the nucleosome-passage rates substantially differ (Fig. 4B). The only difference between the two configurations is the substrate downstream of the nucleosome that Pol II first encounters: naked DNA for the single-nucleosome template and chromatin fiber for the chromatin template. Our previous studies show that the torsional stiffness of chromatin fiber is about 8.5 times softer than that of naked DNA (*61*). The torsional stiffness reduction ultimately results from the left-handed chirality of a nucleosome with DNA wrapping around a histone octamer in a left-handed configuration, constraining (−) supercoiling within a nucleosome (*61*, *84*), with the entry and exit DNA segments being able to adopt different states. Under no torsion, these

segments are more prone to adopt a (−) crossed state. The presence of (+) torsion converts these segments into a (+) crossed state (*62*, *85*), limiting twist buildup without histone dissociation (*61*) (fig. S8). Thus, the torsional mechanical properties of chromatin allow effective buffering of transcription-generated torsional stress on the chromatin template, facilitating transcription through the nucleosome. In contrast, the naked DNA of the single-nucleosome template cannot effectively buffer transcription-generated torsional stress, making torsional stress a significant obstacle to transcription. In a way, this is akin to Pol II twisting substrates of different physical properties: while it is easier to twist chromatin by adding some turns (imagine twisting a rope), it is considerably harder to twist naked DNA by adding the same number of turns (imagine twisting a metal rod) (*5*).

Consistent with this chromatin torsional-mechanical explanation, our measured nucleosome-passage rate is greater on the chromatin template than on the single-nucleosome template by 5.5 ± 0.7 (mean ± SEM) fold with TFIIS and 31.2 ± 7.9 (mean ± SEM) fold without TFIIS (Fig. 4B). Using the torsional mechanical properties of chromatin (*61*), we estimate that Pol II experiences only 1.6 pN·nm resisting torque when encountering a nucleosome on the chromatin template but 8.5 pN·nm resisting torque when encountering a nucleosome on the single-nucleosome template (Fig. 4B, Materials and methods, and fig. S11). To further evaluate this possibility, we also examined the nucleosome-passage rate on a single-nucleosome template that is not torsionally constrained so that torsional stress cannot accumulate on this template (0 pN·nm) (Fig. 4B and figs. S12 and S13). Indeed, the nucleosome-passage rate on this template is substantially increased and even greater than that on the chromatin-fiber template under torsional stress (Fig. 4B), further demonstrating how torsional stress can impact the nucleosome-passage rate.

Collectively, our findings demonstrate the effectiveness of chromatin in buffering torsional stress during transcription. This buffering results from the left-handed nucleosome chirality and does not require the disassembly of nucleosomes downstream of Pol II (*61*) (fig. S8). Although chromatin has been traditionally viewed as a roadblock to transcription, our results show that by buffering torsional stress, chromatin actually facilitates transcription, revealing a crucial role of chromatin in regulating transcription. Although DNA supercoiling and torsional stress are distinct physical quantities, they are often conflated in the literature. Our work shows how torsional stress can significantly impact transcription even under the same degree of supercoiling. Torsional stress (reflected by torque), not DNA supercoiling, dictates the difficulty of Pol II in twisting DNA. The distinction between DNA supercoiling and torsional stress is critical but historically overlooked. Our data help highlight this difference.

**Torsional stress modulates nucleosome passage**

Even though chromatin is an effective torsional buffer, continuous transcription eventually generates enough torsional stress to exceed the buffering capacity of chromatin, limiting Pol II's ability to transcribe through multiple nucleosomes. Thus, timely torsional relaxation by topoisomerases is crucial to ensure Pol II progression (*15*, *19*–*26*). Since topoisomerases relax DNA supercoiling, they should reduce torsion in chromatin and facilitate the passage of Pol II through nucleosomes.

To investigate how topoisomerase relaxation facilitates transcription through chromatin, we conducted transcription experiments in the presence of human topoisomerase I (topo I) or yeast topoisomerase II (topo II) (Fig. 5A) using a configuration similar to that shown in Fig. 3A. Our control experiments show that both topo I and topo II can effectively relax torsional stress in a chromatin substrate (fig. S14) (*61*, *62*). However, the Pol II location on DNA can no longer be tracked in real-time by the DNA extension, because the DNA extension can be altered by topoisomerase relaxation or Pol II translocation and thus does not uniquely inform the Pol II location on the template. Instead, we assess the Pol II location using the extension-turns relation of the chromatin substrate downstream of Pol II. Previously, we have characterized how the width and height of the extension-turns relation of chromatin depend on the number of nucleosomes (*61*, *62*). We now use this characterization to estimate the number of nucleosomes on the remaining chromatin between Pol II and the coverslip, which provides an estimate of the location of Pol II on the template (Materials and methods). As Pol II progresses through nucleosomes, the chromatin array ahead of Pol II shortens, leading to a reduced width and height of the extension-turns relation (Fig. 5B). These features provide an estimation for the number of nucleosomes transcribed.

Using this method, we monitored how Pol II transcribes through chromatin as a function of time (Fig. 5C). In the absence of any topoisomerases, Pol II can transcribe through one nucleosome, consistent with chromatin effectively buffering torsional stress during transcription. However, after the passage of this nucleosome, Pol II significantly slows down while transcribing through the second nucleosome, consistent with torsional stress approaching the buffering capacity of chromatin (fig. S11) and suggesting that further transcription requires torsional relaxation by topoisomerases. Indeed, when either topo I or topo II is present, Pol II can continue to transcribe through multiple nucleosomes with less indication of being significantly slowed down over time. Topo I is more effective in allowing more efficient nucleosome bypass. Thus, the presence of topoisomerases ensures more processive transcription.

In vivo, Pol II may also encounter other motor proteins

that share the same DNA substrate, and Pol II progression is modulated by torsional stress generated by those processes (fig. S15). For example, when one Pol II trails another Pol II moving co-directionally, the leading Pol II generates (−) supercoiling behind that annihilates the (+) supercoiling in front of the trailing Pol II, reducing the torsional stress in front of the trailing Pol II. Similarly, when a Pol II encounters another Pol II or a replisome moving head-on, (+) supercoiling accumulates between the two motors, increasing the torsional stress.

To investigate how additional torsional stress impacts transcription, we allowed Pol II to transcribe on the chromatin template while either mechanically unwinding the DNA to reduce torsional stress or overwinding the DNA to increase torsional stress, mimicking the torsional action of other motor proteins. In this experiment, we rotated the magnet at a constant rate while monitoring the progression of Pol II through a nucleosome (Fig. 5D). As expected, unwinding the chromatin substrate facilitates Pol II progression through a nucleosome while overwinding the chromatin substrate hinders its progress (Fig. 5, D and E). Therefore, the ability of Pol II to bypass a nucleosome is modulated by the level of the torsional stress.

Taken together, these results further highlight the role of torsional stress during transcription through nucleosomes and provide additional support for the torsional mechanical model of transcription. We found that topoisomerase relaxation of torsional stress can significantly facilitate transcription through chromatin, allowing Pol II to progress through multiple nucleosomes without significant hindrance from the torsional stress buildup. We also show that Pol II passage through a nucleosome can be modulated by additional torsional stress, which could be imposed by other motors on the same substrate. These results demonstrate how torsional stress can modulate transcription through nucleosomes.

## Discussion

Our findings show that torsional stress is a strong regulator of transcription through chromatin. We have provided unprecedented information on Pol II transcription dynamics through chromatin under torsion. This work shows a complex interplay of DNA supercoiling generated by Pol II and chromatin's ability to buffer the resulting torsional stress. The direct comparison of transcription through a nucleosome on a single-nucleosome template and a chromatin template also calls attention to the crucial distinction between DNA supercoiling and torsional stress, which have often been conflated in the literature.

We visualized Pol II rotation of DNA, demonstrating the inevitable consequence of torsional stress associated with transcription (Fig. 1, A and B). Although RNAP has primarily been examined as a linear motor that generates force to translocate along the DNA (*46*, *47*, *49*, *51*), this work on Pol II, together with previous studies of *E. coli* RNAP (*13*, *14*), brings to the fore that RNAP is also a rotary motor that generates torques to rotate the DNA. We found that Pol II can generate a torque of about 9 pN·nm that nearly melts the DNA and becomes significantly more powerful in the presence of TFIIS to about 13 pN·nm (Fig. 1 and Fig. 2). Thus, Pol II is a potent rotary motor with its torsional capacity modulated by transcription factors. While this work focuses on the basal transcription machinery with TFIIS, other factors (*49*, *50*, *77*, *86*) will likely further modulate the torsional capacity of Pol II in vivo.

Our data demonstrate that chromatin can effectively buffer (+) torsional stress generated ahead of transcription, allowing Pol II to progress more efficiently through a nucleosome, a feat unattainable if the downstream is naked DNA (Fig. 3 and Fig. 4). Although chromatin has been previously proposed to serve as a buffer of torsional stress (*61*, *85*, *87*, *88*), our data provide experimental evidence that supports this hypothesis in the context of transcription and demonstrates the role of chromatin beyond being just an obstacle. this (+) torsional buffering results from the nucleosome chirality and does not require nucleosome disassembly (*61*, *62*, *85*) (fig. S8). Thus, the left-handed nucleosome chirality coordinates with the right-handed DNA to buffer (+) torsional stress and facilitate transcription through nucleosomes. Genomics studies show that nucleosomes are present within gene bodies at high occupancy, even for highly transcribed genes (*89*, *90*), and deletion of factors that preserve nucleosome integrity on the chromatin could result in a down-regulation of genic transcription (*91*). Thus, chromatin may be a necessary substrate constituent to limit torsional stress accumulation during active transcription.

Previous in vivo studies also show that transcription-generated (+) torsional stress could promote destabilization of nucleosomes ahead of Pol II (*21*, *92*), since each nucleosome traps about one (−) turn by the left-handed wrapping of DNA around a nucleosome (*84*). We previously found that +19 pN·nm can facilitate the dissociation of the H2A/H2B dimers in a nucleosome (*93*), suggesting that the torque generated by Pol II in this work may not be sufficient to disassemble nucleosomes. Our control experiment shows that nucleosomes remain stable during the measurement time under a torque comparable to that generated by Pol II during transcription through a nucleosome (fig. S8). Although Pol II-generated (+) torsion is insufficient to disassemble nucleosomes in our experiments, it could still help to destabilize the nucleosomes ahead of Pol II. In vivo, Pol II could generate greater (+) torsion by interacting with other elongation factors, enhancing its ability to destabilize nucleosomes. In addition, nucleosome remodelers and chaperones could also slide and destabilize the nucleosomes, along with the

assistance of (+) torsion, to allow Pol II passage (*94*, *95*).

We also demonstrate that topo I or topo II can significantly facilitate transcription through multiple nucleosomes (Fig. 5, A to C). Topo I is more effective than topo II in this role. This difference may reflect how each enzyme interacts with its substrate. While topo II relaxes DNA via a strand passage mechanism (*96*) and prefers binding to a DNA crossover (*97*, *98*), topo I relaxes DNA by interacting with a single DNA segment (*99*). On a chromatin substrate, topo II can bind to a crossover formed by the juxtaposition of the entry and exit DNA segments of a nucleosome. However, (+) torsion at a nucleosome first displaces the entry and exit DNA segments before bringing them together into juxtaposition. This leads to fewer DNA crossings being available for topo II binding until significant (+) torsion buildup occurs, and thus a delayed action of topo II in assisting transcription through nucleosomes. This is consistent with our previous finding that topo II has a faster relaxation rate and is more processive on chromatin under high (+) torsion stress (*62*). In contrast, topo I may perform its function by simply binding to the linker DNA between nucleosomes without the need to capture a crossover, thus allowing for more rapid and processive supercoiling relaxation. In support of this interpretation, previous in vivo studies show that topo I is the primary enzyme for relaxing transcription-generated torsional stress (*21*, *92*), and topo I, but not topo II, acts within gene bodies (*21*, *26*). Furthermore, as the torsion increases with the level of transcription, both topo I and topo II enrichment levels also rise, suggesting that torsion might facilitate topoisomerase recruitment or retention (*26*). In addition to topoisomerases, other motors in the vicinity can further modulate torsional stress (*18*). We further show that transcription through chromatin can be up-regulated by (−) torsion or down-regulated by (+) torsion downstream of Pol II for the range of supercoiling introduced in Fig. 5F.

While the torque capacity of Pol II may facilitate transcription against torsional resistance, this property may also exacerbate conflicts with other motor proteins. For example, when Pol II encounters a replisome head-on, (+) torsional stress accumulates between Pol II and the replisome, which could occur well before Pol II physically encounters the replisome since torsional stress can act over a distance. Previous studies support a model in which (+) torsional stress accumulation is the culprit for replication stress, leading to replication fork stalling and disassembly (*29*–*31*). Although the replisome often ultimately wins the conflict (*100*), Pol II's ability to move forward against strong torsional stress will allow a greater (+) torsional buildup between the two motors that leads to greater fork instability, which is detrimental to genome integrity.

Despite chromatin being traditionally viewed as a hindrance to fundamental DNA processes, our findings demonstrate a role of chromatin in promoting transcription through a nucleosome under torsion. Previously, we provided evidence that chromatin facilitates replication by partitioning supercoiling behind the replication fork, simplifying the topology for subsequent chromosome segregation (*61*). This work extends this idea in the context of transcription. These studies reveal the crucial role of chromatin's torsional mechanical properties in fundamental DNA processes.

## Materials and methods

### *Protein expression and purification*

Yeast Pol II containing a 6×His-tag and a biotin tag on both Rpb1 and Rpb3 subunits was expressed and purified from *S. cerevisiae* (*101*). In brief, cell pellets were lysed and went through a HisTrap HP column (Cytiva 17524801), a heparin column (Cytiva 17040703) and a Mono Q column 10/100 (Cytiva 17516701). The resulting product was then biotinylated by GST-BirA and the reaction mixture was slowly loaded to a Mono Q column 5/50 (Cytiva 17516601). The eluted biotinylated Pol II was then checked by SDS-PAGE (fig. S2), concentrated, and flash-frozen for storage.

*S. cerevisiae* recombinant TFIIS was expressed in *BL21 (DE3) pET15b PPR1* (69450-M; Novagen-sigma) (*102*). Cell pellets harvested by centrifugation were sonicated using a microprobe tip and Sonicator-Ultrasonic Processor VHX 750 W (model GEX 750; PG Scientific). The centrifugated lysate was loaded/passed through a HisTrap FF Crude (Cytiva 17528601) and later was loaded to a Mono S column 10/100 GL (Cytiva 17516901). The protein eluted from the column was diluted and reloaded to a HisTrap HP (Cytiva 29051021) column and a Mono S column 5/50 GL (Cytiva 17516801) to produce 6×His-tagged protein. The protein was then checked by SDS-PAGE (fig. S2), concentrated, and flash-frozen for storage.

Human HeLa histones were purified from nuclear pellets of HeLa-S3 (National Cell Culture Center HA.48) cells, followed by a hydroxyapatite Bio-gel HTP gel slurry (Bio-Rad Laboratories) purification (*103*–*105*). The protein was then checked by SDS-PAGE (fig. S2), concentrated, and flash-frozen for storage.

Human topoisomerase I (His-MBP-prescission-hsTOP1, simply topo I) was expressed in High Five insect cells. Cells were collected and resuspended in Buffer A (50 mM HEPES-NaOH pH 7.5, 1 M NaCl, 20 mM imidazole, 5% glycerol, 5 mM βME, 1 mM PMSF, 1 μg/mL Leupeptin and 1 μg/mL Pepstatin). Resuspended cells were lysed by sonication and clarified by centrifugation, followed by application of the clarified lysate to a HisTrap-HP column (Cytiva 17524801) equilibrated in Buffer B (35 mM Tris-HCl pH 7.8, 1 M NaCl, 15 mM imidazole, 5% glycerol, 0.5 mM TCEP, 1 mM PMSF, 1 μg/mL Leupeptin and 1 μg/mL Pepstatin). Captured protein was eluted with Buffer C (35 mM Tris-HCl pH 7.8, 100 mM

NaCl, 300 mM imidazole, 5% glycerol and 0.5 mM TCEP) directly onto a HiTrap-SP sepharose cation exchange column (Cytiva 17515701) equilibrated in Buffer D (35 mM Tris-HCl pH 7.8, 100 mM NaCl and 0.5 mM TCEP) and eluted by a gradient of 0-100% Buffer E (35 mM Tris-HCl pH 7.8, 1 M NaCl and 0.5 mM TCEP). Peak fractions containing His-MBP-prescission-hsTOP1 from ion exchange were pooled and the MPB tag removed by addition of rhinovirus 3C protease. Topo I was further purified by size exclusion chromatography using a Superdex 200 Increase 10/300 GL (Cytiva 28990944) equilibrated in Buffer F (50 mM Tris-HCl pH 7.8, 500 mM KCl, 10% glycerol and 0.5 mM TCEP). Peak fractions containing purified topo I were pooled and brought to a final glycerol concentration of 30%, checked by SDS-PAGE (fig. S2) and flash frozen for storage.

Yeast topoisomerase II (topo II) was expressed in *S. cerevisiae* (*61*–*63*). In brief, cell pellets harvested by centrifugation were lysed, and went through a HisTrap HP column (Cytiva 17524802) and a HiTrap SP HP column (GE 17115201). The protein eluted from the column was concentrated and incubated with TEV protease (QB3 Macro Lab) overnight, removing the 6×His-tag to produce tag-free proteins. The protein was further purified using a HisTrap HP column (Cytiva 17524802) and a Sephacryl column (GE Healthcare). The protein was then checked by SDS-PAGE (fig. S2), concentrated, and flash-frozen for storage.

### *DNA template construction*

The "gapped" DNA construct (fig. S3) was formed on a 0.6 kb DNA PCR amplified from pMDW139 (see table S1 for primer sequences). Two nicks on the non-template strand (NTS) were introduced by Nt.BbvCI (NEB R0632). The sample was then melted and re-annealed with the addition of 40× amount of a DNA oligo with an identical sequence to the template strand (TS) (ARP78 TS in table S1) and went through spin column purification (Select-a-Size DNA Clean & Concentrator, Zymo Research D4080), resulting in a 76 nt gap on the non-template strand. The sample was further digested with BstXI (NEB R0113) to create a unique overhang to ligate to the downstream template.

A second "gapped" DNA construct of 133 bp used for the Pol II upstream torque was formed by annealing three DNA oligos: Upstream NTS, Downstream NTS and Short TS (see table S1 for sequences). The resulting DNA segment contains two unique overhangs at the template ends.

The 5.7 kb DNA construct (fig. S4) for Pol II rotation tracking and downstream stall torque measurement is composed of a 4.6 kb center segment (~50% GC content) flanked by a 0.6 kb transcription elongation complex (TEC) segment and a 0.5 kb multi-digoxigenin-labeled tethering adapter. The 4.6 kb center segment was PCR amplified from pRL574 (see table S1 for primer sequences) with LongAmp Taq (NEB M0534) and digested with BstXI (NEB R0113) and BsaI-HFv2 (NEB R3733) to produce unique overhangs.

The 11.6 kb DNA construct (fig. S4) for Pol II upstream stall torque measurement is composed of a 0.5 kb multi-digoxigenin-labeled tethering adapter, a 6.5 kb upstream segment (~50% GC content), a 133 bp TEC segment and a 4.6 kb center segment. The 6.5 kb upstream segment was PCR amplified from pMDW133 (see table S1 for primer sequences) and digested with BssSI-v2 (NEB R0680) and PpuMI (NEB R0506) to produce unique overhangs.

The 601 sequence (*106*) was used as the nucleosome positioning element (NPE) for both single-nucleosome and nucleosome array templates. The 13.8 kb single-nucleosome template (Fig. 3A) is composed of a 0.6 kb TEC segment, a 0.3 kb nucleosome segment containing a single NPE, a 12.3 kb center segment, and a 0.5 kb multi-digoxigenin-labeled tethering adaptor (*41*, *61*). The reverse PCR primer of the 0.6 kb TEC segment was modified (0.6 kb gapped PCR R Nuc; table S1) to produce the correct overhang for downstream ligation. The 0.3 kb NPE segment was PCR amplified from pMDW2 (see table S1 for primer sequences). The product was then digested with AlwNI (NEB R0514) and BbsI-HF (NEB R3539) to generate overhangs for further ligation. The 12.3 kb center segment was PCR amplified with Phusion (NEB M0530) from λ-DNA (NEB N3011, see table S1 for primer sequences) and digested with BstXI (NEB R0113) and BsaI-HFv2 (NEB R3733) to generate unique overhangs for further ligation.

The 13.8 kb nucleosome array template (Fig. 3A) is composed of a 0.6 kb TEC segment, a 12.7 kb 64-mer segment containing 64 tandem repeats of 197 bp (147 bp NPE + 50 bp linker DNA), and a 0.5 kb multi-digoxigenin-labeled tethering adaptor. The 64-mer segment was digested with FastDigest BglI (Thermo Scientific FD0074) and FastDigest BstXI (Thermo Scientific FD1024) from pMDW72 and went through gel extraction (*61*, *62*).

### *Pol II elongation complex formation*

Pol II was directly assembled into a transcription elongation complex (TEC) (*68*, *69*, *107*). A "gapped" DNA construct was formed with a 76 nt gap on the non-template strand (NTS) (fig. S3). A 14 nt RNA (RNA 14; table S1) was annealed to the gapped region, forming an RNA-DNA hybrid. Pol II was added to the hybrid, followed by the addition of a 76 nt non-template strand DNA oligo (ARP77 NTS; table S1) complementary to the gapped sequence. The nicks at the two ends of the gap were ligated by T4 DNA Ligase (NEB M0202).

### *Nucleosome assembly*

Nucleosomes were assembled using the purified HeLa histones onto DNA constructs via salt dialysis (*61*, *103*–*105*). The NaCl concentration during the dialysis was decreased from 2.0 M to 0. The quality of the assembly was initially assessed

by gel electrophoresis. For single-nucleosome constructs, the quality of the assembled nucleosome was later rigorously assessed with an unzipping assay using optical tweezers (*108*). For nucleosome array constructs, the quality and occupancy of the assembled nucleosomes were later rigorously assessed with a stretching assay using optical tweezers (*61*, *103–105*).

***Experimental conditions***

The assembled Pol II transcription elongation complex was stored in TEC storage buffer (25 mM Tris-HCl pH 8, 150 mM KCl, 1 mM $MgCl_2$, 10 μM $ZnSO_4$, 1.5 mg/mL β-casein, 1 mM DTT, 2 mM TCEP, 3% glycerol). Transcription was resumed by the addition of 1 mM of each ribonucleoside triphosphate (NTPs, Roche 11277057001) in the transcription buffer (25 mM Tris-HCl pH 8, 150 mM KCl, 5 mM $MgCl_2$, 1 mM NTPs, 10 μM $ZnSO_4$, 1.5 mg/mL β-casein, 1 mM DTT, 2 mM TCEP, 3% glycerol). For experiments requiring TFIIS, 500 nM TFIIS was added to the transcription buffer. For experiments requiring topoisomerases, 150 pM human topo I or 100 pM yeast topo II was added to the transcription buffer. All experiments were performed at room temperature.

***Single-molecule assay on angular optical trap (AOT)***

Experiments described in Fig. 1 using the AOT (*13*, *14*, *109*) were performed with the biotinylated Pol II being torsionally anchored on the surface of the chamber via biotin-streptavidin interaction, and the downstream multi-digoxigenin-labeled tethering adaptor being torsionally anchored to the bottom surface of an anti-digoxigenin coated quartz cylinder. To enable this measurement, we modified our previous methods for nanofabrication of the quartz cylinders (*38*, *41*, *61*) before subsequently coating the cylinders with anti-digoxigenin (fig. S1).

These experiments were performed in nitrocellulose-coated sample chambers (*61–63*). The surfaces were functionalized with biotinylated bovine serum albumin (Thermo Scientific 29130) and streptavidin (Agilent SA10-10), then passivated with β-casein (Sigma C6905). DNA was tethered to the surface via Pol II before the quartz cylinders were introduced to the chamber. The laser power entering the objective during all AOT experiments was kept at 20 mW to minimize the possibility of photo-damage.

During the Pol II rotation experiments (Fig. 1B), transcription was resumed by introducing 1 mM NTPs in the transcription buffer. The DNA construct was mechanically unwound until (−) supercoiled plectonemes were formed under a force clamp of 0.3 pN by modulating the trap height. This step encourages Pol II to resume transcription and identifies active Pol II tethers. Continued Pol II transcription neutralized the downstream (−) supercoiling and buckled the DNA to form a (+) plectoneme. After (+) plectoneme formation, the force was clamped at 0.2 pN by mechanical rotation of the cylinder while the extension of the tether was kept constant. Thus, the rotation of the cylinder directly reflects the turns introduced by Pol II transcription. Because this treatment does not take into account the contour length shortening, the measured rotation rate is accurate within ~3%.

During the Pol II stall torque measurement (Fig. 1C), transcription was resumed as above. After Pol II transcription buckled the DNA while working against a resisting torque, the force clamp was turned off, and the trap height was held constant. The cylinder's angular orientation was also held constant to allow accumulation of supercoiling in the DNA. As Pol II transcribed, the force and the corresponding buckling torque (fig. S5) increased until Pol II stalled. The stall torque for each trace is defined as the maximum torque measured within 60 s after the start of stalling. Pol II position along the DNA during the measurement was determined based on the torsional mechanics of the remaining DNA (*13*, *14*, *110*). This stall time duration is greater than or comparable to what we have used previously (*13*, *14*, *47*).

***Single-molecule assay on magnetic tweezers (MT)***

Experiments described in Figs. 2 to 5 were performed with the biotinylated Pol II being torsionally anchored on the surface of a streptavidin-coated magnetic bead, and the downstream multi-digoxigenin-labeled tethering adaptor being torsionally anchored on the surface of the chamber. Sample chambers were assembled as described above for AOT experiments. The surfaces of the assembled sample chambers were functionalized with anti-digoxigenin (Vector Labs MB-7000), and passivated with β-casein (Sigma C6905). About 20 pM DNA constructs were introduced into the chamber, followed by incubation with magnetic beads (Invitrogen 65601).

MT experiments were performed on a home-built instrument (*61–63*), which permits simultaneous measurements of multiple molecules under a constant force. In each sample chamber, the extensions of ~50 actively transcribing Pol IIs were simultaneously measured to determine the position of the Pol II. Although the MT instrument cannot directly measure the torque, the torque can be inferred from the force after the DNA construct has buckled to form plectonemes using the well-established relation between force and torque in plectonemic DNA (*13*, *14*, *61*) (fig. S5).

In the torque-jump assay (Fig. 2A), after the introduction of 1 mM NTPs, the DNA tethers were (−) supercoiled by adding −17 turns under 0.3 pN force to encourage Pol II to resume transcription and identify active Pol II tethers. Pol II was allowed to transcribe for 15-40 s, neutralizing the downstream (−) supercoiling and forming a (+) plectoneme, corresponding to the low torque $\tau_{low}$ = 6 pN·nm. The torque was then rapidly increased from the low torque $\tau_{low}$ to a high torque $\tau_{jump}$, and transcription was monitored for 15 min. For $\tau_{jump}$ = 4 pN·nm, $\tau_{low}$ = 4 pN·nm was used. The pause-free

velocity shown in Fig. 2D is the average of pause-free velocities of individual traces under the indicated torque values. Since the ability to identify pauses relies on the measurement's resolution, some pauses of short extent and/or short duration, which can result from off-pathway states, may be unscored. This may somewhat underestimate the velocity along the main pathway of polymerase elongation. The active fraction of Pol II $f_{active}$ (Fig. 2E) is the ratio of the number of traces active after the torque jump to the total number of traces active before the torque jump. The $f_{active}$ versus $\tau_{jump}$ plot is fit with:

$$f_{active} = \frac{1}{1+\exp\left(\frac{\tau_{jump}-\tau_c}{\tau_0}\right)}$$

which determined the values of $\tau_c$ and $\tau_0$. The critical torque $\tau_c$, at which $f_{active}$ = 0.5, provides a measure of the stall torque (*13*).

In assays probing Pol II transcription through nucleosome substrates (Fig. 3 and Fig. 4), the position of the Pol II was monitored under 0.5 pN force. Before starting transcription, the initial extension versus magnet turns curve (extension-turns curve) of a tether was measured. Immediately after the introduction of 1 mM NTPs and 500 nM TFIIS (if any), the magnet was unwound by –18 turns to encourage Pol II to resume transcription and identify active Pol II tethers. The extension signal was then monitored for 20 min (Fig. 3C), during which Pol II transcription neutralized the downstream (–) supercoiling, introduced (+) supercoiling, and then encountered a nucleosome. After allowing transcription for 20 min, a final (post-transcription) extension-turns curve was measured.

Torsionally unconstrained tethers are present in all sample chambers during the MT measurements. This could occur if a single-tag (instead of a multi-tag) binds to the surface of a bead or coverslip, or if the DNA is nicked. For these tethers, Pol II experiences no torsional stress during elongation. These tethers can be identified by examining the extension-turns curve mentioned above. If the extension remains unchanged during such tether winding, the tether is identified as torsionally unconstrained.

For the topoisomerase assay (Fig. 5, A to C), at the end of a transcription measurement, topo activity was stopped by flushing the chamber with TEC storage buffer just before the measurement of the post-transcription extension-turns curve. Since the shape of the extension-turns curve indicates the number of nucleosomes downstream of Pol II, we use the change in the shape of the extension-turns curve to determine the number of nucleosomes transcribed. Each extension-turns curve is treated as a combination of those of the naked DNA and nucleosome array, based on the lengths of DNA in the naked DNA region and the nucleosomal DNA region. As such, comparing the post-transcription extension-turns curve with the pre-transcription extension-turns curve indicates the nucleosome number change downstream of Pol II, providing the number of nucleosomes Pol II transcribes through.

For torsional modulation assays (Fig. 5, D to F), the magnet was mechanically wound at the indicated rate during the 20-min observation.

### *Pol II position during transcription through a nucleosome*

For MT experiments, the position of Pol II on the template is determined by the contour length of DNA between the Pol II and the magnetic bead. The contour length of DNA must be determined from the measured quantities of force, extension, and number of turns mechanically introduced. This conversion can be made using the mechanical properties of the supercoiled DNA and chromatin (*61*, *62*) with the two constraints. The first is that Pol II tightly tracks the DNA helical groove, resulting in Pol II rotating DNA by one turn for each 10.5 bp transcribed (*2*). The second one is that each nucleosome constrains –1 turn in the 147 bp DNA (*84*, *111*).

Given these constraints, DNA extension during transcription can be converted to the Pol II position along the template as long as the extension-turns curve before transcription is measured (figs. S5 and S9A). This curve was measured for each tether. If a trace did not pause encountering the first NPE, we interpreted it as the NPE being vacant and excluded it from further analysis. For each remaining trace, at a given Pol II position on the template, the expected extension-turns curve is scaled from this initial extension-turns curve based on the DNA and nucleosomes in the remaining template. If a Pol II position is associated with DNA in a nucleosome, the expected extension-turns curve is obtained via a linear interpolation of the curve when Pol II encounters the nucleosome and the curve when Pol II exits the nucleosome. Therefore, as Pol II continues to transcribe, the expected extension-turns curve decreases in the overall height and overall width. Importantly, the curve also shifts to the left due to the accumulation of Pol II generated (+) supercoiling in the DNA.

For Pol II transcribing through a nucleosome under no torsion (torsionally unconstrained tethers), the contour length downstream of the polymerase can be directly inferred by the tether extension (figs. S12 and S13). We assume the contribution of a nucleosome is negligible to the downstream extension. The position of Pol II outside of the nucleosomal region can thus be directly obtained from the downstream contour length. This assay has no resolution of Pol II position inside a nucleosome. Pol II position inside the nucleosome is estimated by an interpolation of Pol II position before and after encountering the nucleosome (fig. S9B).

### *Pol II dwell time encountering a nucleosome*

We aim to find Pol II dwell time when Pol II encounters a nucleosome using the measured Pol II position-time trajectories. Pol II backtracks when experiencing high resisting torque (Fig. 2B) and encountering nucleosomes (Fig. 3C). The extent of such reverse motion occurs at a wide range, adding noise to the signal. Thus, we employed a "first passage" method for processing Pol II trajectories prior to generating the average Pol II position and dwell-time histograms (Fig. 3D, Fig. 4, and Fig. 5E). For every measured Pol II transcribed distance trajectory $x(t)$, we used the maximum distance transcribed $X(t) = \max\left\{x(t_0)\big|_{t_0 \le t}\right\}$. This method mimics the transcript length observed by gel electrophoresis, especially in the absence of TFIIS. Only traces that have reached the dyad are considered for this analysis.

### *Mean trajectory of Pol II*

The mean trajectory of Pol II is determined by pooling many individual traces of Pol II (Fig. 2C, Fig. 4A, and Fig. 5E). For an ensemble of traces with individual Pol II trajectories $\{x_i(t)\}_{i=1,2,3\ldots}$, the mean trajectory is given by $\langle x\rangle(t) = \langle x_i(t)\rangle_{i=1,2,3\ldots}$. For a nucleosome encounter (Fig. 4A, Fig. 5E, and figs. S12 and S13), all individual traces $x_i(t)$ were aligned so that Pol II first encounters the nucleosome at $t$ = 0.

When no torsion was present on a single-nucleosome template (fig. S13), once Pol II passed through the only nucleosome on the template and entered the downstream naked DNA region, it translocated at a greater velocity compared to in the nucleosome region. In this case, the trajectories of individual traces downstream of the nucleosome would greatly impact the average trajectory. As such, we applied a "periodic boundary condition" to minimize averaging bias. For a single Pol II position-time trajectory $x(t)$ (aligned so that Pol II first reaches the nucleosome at $t$ = 0) where Pol II exits the first 197 bp (147 bp NPE + 50 bp downstream linker) at $t_e$, the "periodic boundary condition" trajectory is given by:

$$x_{\mathrm{PBC}}(t) = x\left(t - \lfloor t/t_e \rfloor t_e\right)$$

The mean trajectory is then determined from these "periodic boundary condition" trajectories. This "periodic boundary condition" was only applied to the average trajectories shown in fig. S12C and fig. S13C.

### *Nucleosome passage rate*

Nucleosome passage rate was introduced to compare Pol II's ability to navigate through the nucleosome roadblock. The nucleosome passage rate is the inverse of the dwell time of Pol II inside the NPE sequence, determined from the mean trajectory. For conditions where Pol II mean trajectory did not completely pass through the NPE sequence during the 20-min observation window (e.g., Fig. 4A, left panel), we approximated the dwell time by applying a linear fit to the mean trajectory.

### *Estimate the torque during Pol II passing through a nucleosome*

When Pol II encounters a nucleosome on a single-nucleosome template (Fig. 3C, left panel), plectonemes form on the downstream naked DNA template. We used the buckling torque of naked DNA (8.5 pN·nm under 0.5 pN) (fig. S11A) as an estimate of the resisting torque Pol II experienced when encountering nucleosome. When Pol II encounters a nucleosome on a chromatin template (Fig. 3C, right panel), the resisting torque is determined by the supercoiling state of the downstream nucleosome array template (*61*). We use the supercoiling state of the downstream template when Pol II is at the dyad (Pol II elongating +477 bp from the TSS, twisting the downstream DNA for +45 turns, of which 18 turns are required to move the (−) supercoiling applied by the magnet). This gives an estimated resisting torque on the downstream nucleosome array template of 1.6 pN·nm.

## REFERENCES AND NOTES


1. R. Bermejo, M. S. Lai, M. Foiani, Preventing replication stress to maintain genome stability: Resolving conflicts between replication and transcription. *Mol. Cell* **45**, 710–718 (2012). doi:10.1016/j.molcel.2012.03.001 Medline
2. J. D. Watson, F. H. C. Crick, Genetical implications of the structure of deoxyribonucleic acid. *Nature* **171**, 964–967 (1953). doi:10.1038/171964b0 Medline
3. J. D. Watson, F. H. C. Crick, The structure of DNA. *Cold Spring Harb. Symp. Quant. Biol.* **18**, 123–131 (1953). doi:10.1101/SQB.1953.018.01.020 Medline
4. J. Ma, M. D. Wang, DNA supercoiling during transcription. *Biophys. Rev.* **8**, 75–87 (2016). doi:10.1007/s12551-016-0215-9 Medline
5. J. L. Killian, J. Ma, M. D. Wang, in *RNA Polymerases as Molecular Motors: On the Road*, R. Landick, T. Strick, J. Wang, Eds. (The Royal Society of Chemistry, ed. 2, 2021), pp. 46–71.
6. F. Kouzine, J. Liu, S. Sanford, H.-J. Chung, D. Levens, The dynamic response of upstream DNA to transcription-generated torsional stress. *Nat. Struct. Mol. Biol.* **11**, 1092–1100 (2004). doi:10.1038/nsmb848 Medline
7. F. Kouzine, S. Sanford, Z. Elisha-Feil, D. Levens, The functional response of upstream DNA to dynamic supercoiling *in vivo*. *Nat. Struct. Mol. Biol.* **15**, 146–154 (2008). doi:10.1038/nsmb.1372 Medline
8. F. Kouzine, D. Levens, L. Baranello, DNA topology and transcription. *Nucleus* **5**, 195–202 (2014). doi:10.4161/nucl.28909 Medline
9. S. Chong, C. Chen, H. Ge, X. S. Xie, Mechanism of transcriptional bursting in bacteria. *Cell* **158**, 314–326 (2014). doi:10.1016/j.cell.2014.05.038 Medline
10. S. Kim, B. Beltran, I. Irnov, C. Jacobs-Wagner, Long-Distance Cooperative and Antagonistic RNA Polymerase Dynamics via DNA Supercoiling. *Cell* **179**, 106–119.e16 (2019). doi:10.1016/j.cell.2019.08.033 Medline
11. A. Revyakin, R. H. Ebright, T. R. Strick, Promoter unwinding and promoter clearance by RNA polymerase: Detection by single-molecule DNA nanomanipulation. *Proc. Natl. Acad. Sci. U.S.A.* **101**, 4776–4780 (2004). doi:10.1073/pnas.0307241101 Medline
12. A. Revyakin, C. Liu, R. H. Ebright, T. R. Strick, Abortive initiation and productive initiation by RNA polymerase involve DNA scrunching. *Science* **314**, 1139–1143 (2006). doi:10.1126/science.1131398 Medline
13. J. Ma, L. Bai, M. D. Wang, Transcription under torsion. *Science* **340**, 1580–1583 (2013). doi:10.1126/science.1235441 Medline
14. J. Ma, C. Tan, X. Gao, R. M. Fulbright Jr., J. W. Roberts, M. D. Wang, Transcription

factor regulation of RNA polymerase's torque generation capacity. *Proc. Natl. Acad. Sci. U.S.A.* **116**, 2583–2588 (2019). doi:10.1073/pnas.1807031116 Medline
15. I. Bermúdez, J. García-Martínez, J. E. Pérez-Ortín, J. Roca, A method for genome-wide analysis of DNA helical tension by means of psoralen-DNA photobinding. *Nucleic Acids Res.* **38**, e182–e182 (2010). doi:10.1093/nar/gkq687 Medline
16. F. Kouzine, D. Levens, The Texture of Chromatin. *Cell* **179**, 579–581 (2019). doi:10.1016/j.cell.2019.09.026 Medline
17. R. K. Jha, D. Levens, F. Kouzine, Mechanical determinants of chromatin topology and gene expression. *Nucleus* **13**, 95–116 (2022). doi:10.1080/19491034.2022.2038868 Medline
18. Y. Pommier, A. Nussenzweig, S. Takeda, C. Austin, Human topoisomerases and their roles in genome stability and organization. *Nat. Rev. Mol. Cell Biol.* **23**, 407–427 (2022). doi:10.1038/s41580-022-00452-3 Medline
19. F. Kouzine, A. Gupta, L. Baranello, D. Wojtowicz, K. Ben-Aissa, J. Liu, T. M. Przytycka, D. Levens, Transcription-dependent dynamic supercoiling is a short-range genomic force. *Nat. Struct. Mol. Biol.* **20**, 396–403 (2013). doi:10.1038/nsmb.2517 Medline
20. C. Naughton, N. Avlonitis, S. Corless, J. G. Prendergast, I. K. Mati, P. P. Eijk, S. L. Cockroft, M. Bradley, B. Ylstra, N. Gilbert, Transcription forms and remodels supercoiling domains unfolding large-scale chromatin structures. *Nat. Struct. Mol. Biol.* **20**, 387–395 (2013). doi:10.1038/nsmb.2509 Medline
21. S. S. Teves, S. Henikoff, Transcription-generated torsional stress destabilizes nucleosomes. *Nat. Struct. Mol. Biol.* **21**, 88–94 (2014). doi:10.1038/nsmb.2723 Medline
22. L. Baranello, D. Wojtowicz, K. Cui, B. N. Devaiah, H.-J. Chung, K. Y. Chan-Salis, R. Guha, K. Wilson, X. Zhang, H. Zhang, J. Piotrowski, C. J. Thomas, D. S. Singer, B. F. Pugh, Y. Pommier, T. M. Przytycka, F. Kouzine, B. A. Lewis, K. Zhao, D. Levens, RNA Polymerase II Regulates Topoisomerase 1 Activity to Favor Efficient Transcription. *Cell* **165**, 357–371 (2016). doi:10.1016/j.cell.2016.02.036 Medline
23. Y. J. Achar, M. Adhil, R. Choudhary, N. Gilbert, M. Foiani, Negative supercoil at gene boundaries modulates gene topology. *Nature* **577**, 701–705 (2020). doi:10.1038/s41586-020-1934-4 Medline
24. M. S. Guo, R. Kawamura, M. L. Littlehale, J. F. Marko, M. T. Laub, High-resolution, genome-wide mapping of positive supercoiling in chromosomes. *eLife* **10**, e67236 (2021). doi:10.7554/eLife.67236 Medline
25. Q. Yao, L. Zhu, Z. Shi, S. Banerjee, C. Chen, Topoisomerase-modulated genome-wide DNA supercoiling domains colocalize with nuclear compartments and regulate human gene expression. *Nat. Struct. Mol. Biol.* **32**, 48–61 (2025). doi:10.1038/s41594-024-01377-5 Medline
26. P. M. Hall, L. A. Mayse, L. Bai, M. B. Smolka, B. F. Pugh, M. D. Wang, High-Resolution Genome-Wide Maps Reveal Widespread Presence of Torsional Insulation. *eLife* **14**, RP105675 (2025). doi:10.7554/eLife.105675.1
27. M. Dunaway, E. A. Ostrander, Local domains of supercoiling activate a eukaryotic promoter *in vivo*. *Nature* **361**, 746–748 (1993). doi:10.1038/361746a0 Medline
28. H. P. Patel, S. Coppola, W. Pomp, U. Aiello, I. Brouwer, D. Libri, T. L. Lenstra, DNA supercoiling restricts the transcriptional bursting of neighboring eukaryotic genes. *Mol. Cell* **83**, 1573–1587.e8 (2023). doi:10.1016/j.molcel.2023.04.015 Medline
29. K. S. Lang, A. N. Hall, C. N. Merrikh, M. Ragheb, H. Tabakh, A. J. Pollock, J. J. Woodward, J. E. Dreifus, H. Merrikh, Replication-Transcription Conflicts Generate R-Loops that Orchestrate Bacterial Stress Survival and Pathogenesis. *Cell* **170**, 787–799.e18 (2017). doi:10.1016/j.cell.2017.07.044 Medline
30. K. S. Lang, H. Merrikh, Topological stress is responsible for the detrimental outcomes of head-on replication-transcription conflicts. *Cell Rep.* **34**, 108797 (2021). doi:10.1016/j.celrep.2021.108797 Medline
31. S. French, Consequences of replication fork movement through transcription units in vivo. *Science* **258**, 1362–1365 (1992). doi:10.1126/science.1455232 Medline
32. Y. Liu, V. Bondarenko, A. Ninfa, V. M. Studitsky, DNA supercoiling allows enhancer action over a large distance. *Proc. Natl. Acad. Sci. U.S.A.* **98**, 14883–14888 (2001). doi:10.1073/pnas.261477898 Medline
33. D. Racko, F. Benedetti, J. Dorier, A. Stasiak, Are TADs supercoiled? *Nucleic Acids Res.* **47**, 521–532 (2019). doi:10.1093/nar/gky1091 Medline
34. J. R. Portman, G. M. Brouwer, J. Bollins, N. J. Savery, T. R. Strick, Cotranscriptional R-loop formation by Mfd involves topological partitioning of DNA. *Proc. Natl. Acad. Sci. U.S.A.* **118**, e2019630118 (2021). doi:10.1073/pnas.2019630118 Medline
35. K. Luger, A. W. Mäder, R. K. Richmond, D. F. Sargent, T. J. Richmond, Crystal structure of the nucleosome core particle at 2.8 Å resolution. *Nature* **389**, 251–260 (1997). doi:10.1038/38444 Medline
36. Y. Harada, O. Ohara, A. Takatsuki, H. Itoh, N. Shimamoto, K. Kinosita Jr., Direct observation of DNA rotation during transcription by *Escherichia coli* RNA polymerase. *Nature* **409**, 113–115 (2001). doi:10.1038/35051126 Medline
37. P. Kosuri, B. D. Altheimer, M. Dai, P. Yin, X. Zhuang, Rotation tracking of genome-processing enzymes using DNA origami rotors. *Nature* **572**, 136–140 (2019). doi:10.1038/s41586-019-1397-7 Medline
38. C. Deufel, S. Forth, C. R. Simmons, S. Dejgosha, M. D. Wang, Nanofabricated quartz cylinders for angular trapping: DNA supercoiling torque detection. *Nat. Methods* **4**, 223–225 (2007). doi:10.1038/nmeth1013 Medline
39. S. Forth, C. Deufel, M. Y. Sheinin, B. Daniels, J. P. Sethna, M. D. Wang, Abrupt buckling transition observed during the plectoneme formation of individual DNA molecules. *Phys. Rev. Lett.* **100**, 148301 (2008). doi:10.1103/PhysRevLett.100.148301 Medline
40. M. Y. Sheinin, S. Forth, J. F. Marko, M. D. Wang, Underwound DNA under tension: Structure, elasticity, and sequence-dependent behaviors. *Phys. Rev. Lett.* **107**, 108102 (2011). doi:10.1103/PhysRevLett.107.108102 Medline
41. X. Gao, Y. Hong, F. Ye, J. T. Inman, M. D. Wang, Torsional Stiffness of Extended and Plectonemic DNA. *Phys. Rev. Lett.* **127**, 028101 (2021). doi:10.1103/PhysRevLett.127.028101 Medline
42. Y. Hong, F. Ye, J. Qian, X. Gao, J. T. Inman, M. D. Wang, Optical torque calculations and measurements for DNA torsional studies. *Biophys. J.* **123**, 3080–3089 (2024). doi:10.1016/j.bpj.2024.07.005 Medline
43. A. La Porta, M. D. Wang, Optical torque wrench: Angular trapping, rotation, and torque detection of quartz microparticles. *Phys. Rev. Lett.* **92**, 190801 (2004). doi:10.1103/PhysRevLett.92.190801 Medline
44. J. Inman, S. Forth, M. D. Wang, Passive torque wrench and angular position detection using a single-beam optical trap. *Opt. Lett.* **35**, 2949–2951 (2010). doi:10.1364/OL.35.002949 Medline
45. X. Jia, X. Gao, S. Zhang, J. T. Inman, Y. Hong, A. Singh, S. Patel, M. D. Wang, Torsion is a Dynamic Regulator of DNA Replication Stalling and Reactivation. bioRxiv 2024.10.14.618227 [Preprint] (2024). doi:10.1101/2024.10.14.618227
46. H. Yin, M. D. Wang, K. Svoboda, R. Landick, S. M. Block, J. Gelles, Transcription against an applied force. *Science* **270**, 1653–1657 (1995). doi:10.1126/science.270.5242.1653 Medline
47. M. D. Wang, M. J. Schnitzer, H. Yin, R. Landick, J. Gelles, S. M. Block, Force and velocity measured for single molecules of RNA polymerase. *Science* **282**, 902–907 (1998). doi:10.1126/science.282.5390.902 Medline
48. K. Adelman, A. La Porta, T. J. Santangelo, J. T. Lis, J. W. Roberts, M. D. Wang, Single molecule analysis of RNA polymerase elongation reveals uniform kinetic behavior. *Proc. Natl. Acad. Sci. U.S.A.* **99**, 13538–13543 (2002). doi:10.1073/pnas.212358999 Medline
49. T. Ishibashi, M. Dangkulwanich, Y. Coello, T. A. Lionberger, L. Lubkowska, A. S. Ponticelli, M. Kashlev, C. Bustamante, Transcription factors IIS and IIF enhance transcription efficiency by differentially modifying RNA polymerase pausing dynamics. *Proc. Natl. Acad. Sci. U.S.A.* **111**, 3419–3424 (2014). doi:10.1073/pnas.1401611111 Medline
50. V. Schweikhard, C. Meng, K. Murakami, C. D. Kaplan, R. D. Kornberg, S. M. Block, Transcription factors TFIIF and TFIIS promote transcript elongation by RNA polymerase II by synergistic and independent mechanisms. *Proc. Natl. Acad. Sci. U.S.A.* **111**, 6642–6647 (2014). doi:10.1073/pnas.1405181111 Medline
51. E. A. Galburt, S. W. Grill, A. Wiedmann, L. Lubkowska, J. Choy, E. Nogales, M. Kashlev, C. Bustamante, Backtracking determines the force sensitivity of RNAP II in a factor-dependent manner. *Nature* **446**, 820–823 (2007). doi:10.1038/nature05701 Medline
52. A. Lisica, C. Engel, M. Jahnel, É. Roldán, E. A. Galburt, P. Cramer, S. W. Grill, Mechanisms of backtrack recovery by RNA polymerases I and II. *Proc. Natl. Acad. Sci. U.S.A.* **113**, 2946–2951 (2016). doi:10.1073/pnas.1517011113 Medline
53. L. F. Liu, J. C. Wang, Supercoiling of the DNA template during transcription. *Proc. Natl. Acad. Sci. U.S.A.* **84**, 7024–7027 (1987). doi:10.1073/pnas.84.20.7024 Medline
54. M. G. Izban, D. S. Luse, Factor-stimulated RNA polymerase II transcribes at physiological elongation rates on naked DNA but very poorly on chromatin

templates. *J. Biol. Chem.* **267**, 13647–13655 (1992). doi:10.1016/S0021-9258(18)42262-4 Medline
55. N. Komissarova, M. Kashlev, Transcriptional arrest: Escherichia coli RNA polymerase translocates backward, leaving the 3′ end of the RNA intact and extruded. *Proc. Natl. Acad. Sci. U.S.A.* **94**, 1755–1760 (1997). doi:10.1073/pnas.94.5.1755 Medline
56. E. Nudler, A. Mustaev, E. Lukhtanov, A. Goldfarb, The RNA-DNA hybrid maintains the register of transcription by preventing backtracking of RNA polymerase. *Cell* **89**, 33–41 (1997). doi:10.1016/S0092-8674(00)80180-4 Medline
57. D. Wang, D. A. Bushnell, X. Huang, K. D. Westover, M. Levitt, R. D. Kornberg, Structural basis of transcription: Backtracked RNA polymerase II at 3.4 angstrom resolution. *Science* **324**, 1203–1206 (2009). doi:10.1126/science.1168729 Medline
58. D. Zatreanu, Z. Han, R. Mitter, E. Tumini, H. Williams, L. Gregersen, A. B. Dirac-Svejstrup, S. Roma, A. Stewart, A. Aguilera, J. Q. Svejstrup, Elongation Factor TFIIS Prevents Transcription Stress and R-Loop Accumulation to Maintain Genome Stability. *Mol. Cell* **76**, 57–69.e9 (2019). doi:10.1016/j.molcel.2019.07.037 Medline
59. S. Sigurdsson, A. B. Dirac-Svejstrup, J. Q. Svejstrup, Evidence that transcript cleavage is essential for RNA polymerase II transcription and cell viability. *Mol. Cell* **38**, 202–210 (2010). doi:10.1016/j.molcel.2010.02.026 Medline
60. T. M. Kay, J. T. Inman, L. Lubkowska, T. T. Le, J. Qian, P. M. Hall, S. Batra, D. Remus, D. Wang, M. Kashlev, M. D. Wang, RNA polymerase II is a polar roadblock to a progressing DNA fork. *Nat. Commun.* **16**, 8631 (2025). doi:10.1038/s41467-025-63662-1 Medline
61. T. T. Le, X. Gao, S. H. Park, J. Lee, J. T. Inman, J. H. Lee, J. L. Killian, R. P. Badman, J. M. Berger, M. D. Wang, Synergistic Coordination of Chromatin Torsional Mechanics and Topoisomerase Activity. *Cell* **179**, 619–631.e15 (2019). doi:10.1016/j.cell.2019.09.034 Medline
62. J. Lee, M. Wu, J. T. Inman, G. Singh, S. H. Park, J. H. Lee, R. M. Fulbright, Y. Hong, J. Jeong, J. M. Berger, M. D. Wang, Chromatinization modulates topoisomerase II processivity. *Nat. Commun.* **14**, 6844 (2023). doi:10.1038/s41467-023-42600-z Medline
63. T. T. Le, M. Wu, J. H. Lee, N. Bhatt, J. T. Inman, J. M. Berger, M. D. Wang, Etoposide promotes DNA loop trapping and barrier formation by topoisomerase II. *Nat. Chem. Biol.* **19**, 641–650 (2023). doi:10.1038/s41589-022-01235-9 Medline
64. E. J. Tomko, J. Fishburn, S. Hahn, E. A. Galburt, TFIIH generates a six-base-pair open complex during RNAP II transcription initiation and start-site scanning. *Nat. Struct. Mol. Biol.* **24**, 1139–1145 (2017). doi:10.1038/nsmb.3500 Medline
65. L. Bai, A. Shundrovsky, M. D. Wang, Sequence-dependent kinetic model for transcription elongation by RNA polymerase. *J. Mol. Biol.* **344**, 335–349 (2004). doi:10.1016/j.jmb.2004.08.107 Medline
66. L. Bai, R. M. Fulbright, M. D. Wang, Mechanochemical kinetics of transcription elongation. *Phys. Rev. Lett.* **98**, 068103 (2007). doi:10.1103/PhysRevLett.98.068103 Medline
67. T. Kujirai, H. Kurumizaka, Transcription through the nucleosome. *Curr. Opin. Struct. Biol.* **61**, 42–49 (2020). doi:10.1016/j.sbi.2019.10.007 Medline
68. M. L. Kireeva, B. Hancock, G. H. Cremona, W. Walter, V. M. Studitsky, M. Kashlev, Nature of the nucleosomal barrier to RNA polymerase II. *Mol. Cell* **18**, 97–108 (2005). doi:10.1016/j.molcel.2005.02.027 Medline
69. M. L. Kireeva, W. Walter, V. Tchernajenko, V. Bondarenko, M. Kashlev, V. M. Studitsky, Nucleosome remodeling induced by RNA polymerase II: Loss of the H2A/H2B dimer during transcription. *Mol. Cell* **9**, 541–552 (2002). doi:10.1016/S1097-2765(02)00472-0 Medline
70. C. Hodges, L. Bintu, L. Lubkowska, M. Kashlev, C. Bustamante, Nucleosomal fluctuations govern the transcription dynamics of RNA polymerase II. *Science* **325**, 626–628 (2009). doi:10.1126/science.1172926 Medline
71. L. Bintu, T. Ishibashi, M. Dangkulwanich, Y.-Y. Wu, L. Lubkowska, M. Kashlev, C. Bustamante, Nucleosomal elements that control the topography of the barrier to transcription. *Cell* **151**, 738–749 (2012). doi:10.1016/j.cell.2012.10.009 Medline
72. V. M. Studitsky, G. A. Kassavetis, E. P. Geiduschek, G. Felsenfeld, Mechanism of transcription through the nucleosome by eukaryotic RNA polymerase. *Science* **278**, 1960–1963 (1997). doi:10.1126/science.278.5345.1960 Medline
73. H. Ehara, T. Kujirai, Y. Fujino, M. Shirouzu, H. Kurumizaka, S. I. Sekine, Structural insight into nucleosome transcription by RNA polymerase II with elongation factors. *Science* **363**, 744–747 (2019). doi:10.1126/science.aav8912 Medline
74. L. Farnung, S. M. Vos, P. Cramer, Structure of transcribing RNA polymerase II-nucleosome complex. *Nat. Commun.* **9**, 5432 (2018). doi:10.1038/s41467-018-07870-y Medline
75. M. Wu, C. Beck, J. H. Lee, R. M. Fulbright Jr., J. Jeong, J. T. Inman, M. V. Woodhouse, J. M. Berger, M. D. Wang, Human Topoisomerase IIα Promotes Chromatin Condensation Via a Phase Transition. bioRxiv 2024.10.15.618281 [Preprint] (2024). doi:10.1101/2024.10.15.618281
76. T. T. Le, X. Gao, S. H. Park, J. Lee, J. T. Inman, M. D. Wang, An Effective Surface Passivation Assay for Single-Molecule Studies of Chromatin and Topoisomerase II. bioRxiv 2024.09.25.614989 [Preprint] (2024). doi:10.1101/2024.09.25.614989
77. H. Ehara, T. Yokoyama, H. Shigematsu, S. Yokoyama, M. Shirouzu, S. I. Sekine, Structure of the complete elongation complex of RNA polymerase II with basal factors. *Science* **357**, 921–924 (2017). doi:10.1126/science.aan8552 Medline
78. M. A. Hall, A. Shundrovsky, L. Bai, R. M. Fulbright, J. T. Lis, M. D. Wang, High-resolution dynamic mapping of histone-DNA interactions in a nucleosome. *Nat. Struct. Mol. Biol.* **16**, 124–129 (2009). doi:10.1038/nsmb.1526 Medline
79. V. A. Bondarenko, L. M. Steele, A. Ujvári, D. A. Gaykalova, O. I. Kulaeva, Y. S. Polikanov, D. S. Luse, V. M. Studitsky, Nucleosomes can form a polar barrier to transcript elongation by RNA polymerase II. *Mol. Cell* **24**, 469–479 (2006). doi:10.1016/j.molcel.2006.09.009 Medline
80. J. Jin, L. Bai, D. S. Johnson, R. M. Fulbright, M. L. Kireeva, M. Kashlev, M. D. Wang, Synergistic action of RNA polymerases in overcoming the nucleosomal barrier. *Nat. Struct. Mol. Biol.* **17**, 745–752 (2010). doi:10.1038/nsmb.1798 Medline
81. L. S. Churchman, J. S. Weissman, Nascent transcript sequencing visualizes transcription at nucleotide resolution. *Nature* **469**, 368–373 (2011). doi:10.1038/nature09652 Medline
82. H. Kwak, N. J. Fuda, L. J. Core, J. T. Lis, Precise maps of RNA polymerase reveal how promoters direct initiation and pausing. *Science* **339**, 950–953 (2013). doi:10.1126/science.1229386 Medline
83. C. M. Weber, S. Ramachandran, S. Henikoff, Nucleosomes are context-specific, H2A.Z-modulated barriers to RNA polymerase. *Mol. Cell* **53**, 819–830 (2014). doi:10.1016/j.molcel.2014.02.014 Medline
84. R. T. Simpson, F. Thoma, J. M. Brubaker, Chromatin reconstituted from tandemly repeated cloned DNA fragments and core histones: A model system for study of higher order structure. *Cell* **42**, 799–808 (1985). doi:10.1016/0092-8674(85)90276-4 Medline
85. A. Bancaud, N. Conde e Silva, M. Barbi, G. Wagner, J.-F. Allemand, J. Mozziconacci, C. Lavelle, V. Croquette, J.-M. Victor, A. Prunell, J.-L. Viovy, Structural plasticity of single chromatin fibers revealed by torsional manipulation. *Nat. Struct. Mol. Biol.* **13**, 444–450 (2006). doi:10.1038/nsmb1087 Medline
86. S.-K. Lee, S.-L. Yu, L. Prakash, S. Prakash, Requirement for yeast *RAD26*, a homolog of the human *CSB* gene, in elongation by RNA polymerase II. *Mol. Cell. Biol.* **21**, 8651–8656 (2001). doi:10.1128/MCB.21.24.8651-8656.2001 Medline
87. S. Brahmachari, S. Tripathi, J. N. Onuchic, H. Levine, Nucleosomes play a dual role in regulating transcription dynamics. *Proc. Natl. Acad. Sci. U.S.A.* **121**, e2319772121 (2024). doi:10.1073/pnas.2319772121 Medline
88. C. Bécavin, M. Barbi, J.-M. Victor, A. Lesne, Transcription within condensed chromatin: Steric hindrance facilitates elongation. *Biophys. J.* **98**, 824–833 (2010). doi:10.1016/j.bpj.2009.10.054 Medline
89. E. Oberbeckmann, M. Wolff, N. Krietenstein, M. Heron, J. L. Ellins, A. Schmid, S. Krebs, H. Blum, U. Gerland, P. Korber, Absolute nucleosome occupancy map for the *Saccharomyces cerevisiae* genome. *Genome Res.* **29**, 1996–2009 (2019). doi:10.1101/gr.253419.119 Medline
90. M. A. Schwabish, K. Struhl, Evidence for eviction and rapid deposition of histones upon transcriptional elongation by RNA polymerase II. *Mol. Cell. Biol.* **24**, 10111–10117 (2004). doi:10.1128/MCB.24.23.10111-10117.2004 Medline
91. K. Žumer, M. Ochmann, A. Aljahani, A. Zheenbekova, A. Devadas, K. C. Maier, P. Rus, U. Neef, A. M. Oudelaar, P. Cramer, FACT maintains chromatin architecture and thereby stimulates RNA polymerase II pausing during transcription *in vivo*. *Mol. Cell* **84**, 2053–2069.e9 (2024). doi:10.1016/j.molcel.2024.05.003 Medline
92. M. Durand-Dubief, J. Persson, U. Norman, E. Hartsuiker, K. Ekwall, Topoisomerase I regulates open chromatin and controls gene expression *in vivo*. *EMBO J.* **29**, 2126–2134 (2010). doi:10.1038/emboj.2010.109 Medline

93. M. Y. Sheinin, M. Li, M. Soltani, K. Luger, M. D. Wang, Torque modulates nucleosome stability and facilitates H2A/H2B dimer loss. *Nat. Commun.* **4**, 2579 (2013). doi:10.1038/ncomms3579 Medline
94. L. Farnung, M. Ochmann, M. Engeholm, P. Cramer, Structural basis of nucleosome transcription mediated by Chd1 and FACT. *Nat. Struct. Mol. Biol.* **28**, 382–387 (2021). doi:10.1038/s41594-021-00578-6 Medline
95. Y. Liu, K. Zhou, N. Zhang, H. Wei, Y. Z. Tan, Z. Zhang, B. Carragher, C. S. Potter, S. D'Arcy, K. Luger, FACT caught in the act of manipulating the nucleosome. *Nature* **577**, 426–431 (2020). doi:10.1038/s41586-019-1820-0 Medline
96. J. Roca, J. C. Wang, The capture of a DNA double helix by an ATP-dependent protein clamp: A key step in DNA transport by type II DNA topoisomerases. *Cell* **71**, 833–840 (1992). doi:10.1016/0092-8674(92)90558-T Medline
97. J. Roca, J. C. Wang, DNA transport by a type II DNA topoisomerase: Evidence in favor of a two-gate mechanism. *Cell* **77**, 609–616 (1994). doi:10.1016/0092-8674(94)90222-4 Medline
98. J. M. Berger, S. J. Gamblin, S. C. Harrison, J. C. Wang, Structure and mechanism of DNA topoisomerase II. *Nature* **379**, 225–232 (1996). doi:10.1038/379225a0 Medline
99. L. Stewart, M. R. Redinbo, X. Qiu, W. G. J. Hol, J. J. Champoux, A model for the mechanism of human topoisomerase I. *Science* **279**, 1534–1541 (1998). doi:10.1126/science.279.5356.1534 Medline
100. T. García-Muse, A. Aguilera, Transcription-replication conflicts: How they occur and how they are resolved. *Nat. Rev. Mol. Cell Biol.* **17**, 553–563 (2016). doi:10.1038/nrm.2016.88 Medline
101. M. L. Kireeva, L. Lubkowska, N. Komissarova, M. Kashlev, in *RNA Polymerases and Associated Factors, Part C*, S. Adhya, S. Garges, Eds., vol. 370 of *Methods in Enzymology* (Academic Press, 2003), pp. 138–155.
102. K. R. Christie, D. E. Awrey, A. M. Edwards, C. M. Kane, Purified yeast RNA polymerase II reads through intrinsic blocks to elongation in response to the yeast TFIIS analogue, P37. *J. Biol. Chem.* **269**, 936–943 (1994). doi:10.1016/S0021-9258(17)42202-2 Medline
103. B. D. Brower-Toland, C. L. Smith, R. C. Yeh, J. T. Lis, C. L. Peterson, M. D. Wang, Mechanical disruption of individual nucleosomes reveals a reversible multistage release of DNA. *Proc. Natl. Acad. Sci. U.S.A.* **99**, 1960–1965 (2002). doi:10.1073/pnas.022638399 Medline
104. B. Brower-Toland, M. D. Wang, in *Chromatin and Chromatin Remodeling Enzymes, Part B*, C. D. Allis, C. Wu, Eds., vol. 376 of *Methods in Enzymology* (Academic Press, 2003), pp. 62–72.
105. B. Brower-Toland, D. A. Wacker, R. M. Fulbright, J. T. Lis, W. L. Kraus, M. D. Wang, Specific contributions of histone tails and their acetylation to the mechanical stability of nucleosomes. *J. Mol. Biol.* **346**, 135–146 (2005). doi:10.1016/j.jmb.2004.11.056 Medline
106. P. T. Lowary, J. Widom, New DNA sequence rules for high affinity binding to histone octamer and sequence-directed nucleosome positioning. *J. Mol. Biol.* **276**, 19–42 (1998). doi:10.1006/jmbi.1997.1494 Medline
107. W. Walter, M. L. Kireeva, V. M. Studitsky, M. Kashlev, Bacterial polymerase and yeast polymerase II use similar mechanisms for transcription through nucleosomes. *J. Biol. Chem.* **278**, 36148–36156 (2003). doi:10.1074/jbc.M305647200 Medline
108. L. D. Brennan, R. A. Forties, S. S. Patel, M. D. Wang, DNA looping mediates nucleosome transfer. *Nat. Commun.* **7**, 13337 (2016). doi:10.1038/ncomms13337 Medline
109. X. Gao, J. T. Inman, M. D. Wang, in *Optical Tweezers: Methods and Protocols*, A. Gennerich, Ed., vol. 2478 of *Methods in Molecular Biology* (Humana, 2022), pp. 37–73.
110. J. Ma, C. Tan, M. D. Wang, in *Molecular Motors: Methods and Protocols*, C. Lavelle, Ed., vol. 1805 of *Methods in Molecular Biology* (Humana Press, 2018), pp. 301–332.
111. V. G. Norton, B. S. Imai, P. Yau, E. M. Bradbury, Histone acetylation reduces nucleosome core particle linking number change. *Cell* **57**, 449–457 (1989). doi:10.1016/0092-8674(89)90920-3 Medline
112. WangLabCornell, WangLabCornell/Qian_et_al: Release_1.0 (Release_1.0), Zenodo (2025). doi:10.5281/zenodo.17419438

## ACKNOWLEDGMENTS

We thank Drs. M. Wu, T.T. Le, S. Park, and J. Lee for help with single-molecule assays of nucleosomes and topoisomerases, Dr. X. Gao for assistance with the AOT maintenance and calibration, and members of the Wang Laboratory and Dr. J.W. Roberts for helpful discussion and comments. **Funding:** This study was supported by the National Institutes of Health grants R01GM136894 (to M.D.W.) and T32GM008267 (to M.D.W.), the Intramural Research Program of the NIH National Cancer Institute (to M.K.), and the National Cancer Institute grant R35CA263778 (to J.M.B.). M.D.W. is a Howard Hughes Medical Institute (HHMI). This work has been performed in part at the Cornell NanoScale Facility, a member of the National Nanotechnology Coordinated Infrastructure (NNCI) supported by the National Science Foundation (Grant NNCI-2025233). **Author contributions:** J.Q. and M.D.W. designed single-molecule assays. J.Q. and S.Z. performed single-molecule experiments. C.T. performed preliminary experiments during the early stage of the project. J.Q. and T.M.K. prepared DNA templates. Y.H. fabricated and calibrated quartz cylinders. X.J. and J.T.I. assisted in the AOT method development. J.Q. and J.T.I. analyzed data. L.L. and M.K. purified and characterized Pol II and TFIIS. D.G. created the yeast strain for Pol II purification. R.M.F. purified and characterized histones. J.J., G.H., and J.M.B. purified and characterized human topo I and yeast topo II. M.D.W. wrote the initial draft. All authors contributed to the manuscript revision. M.D.W. supervised the project. **Competing interests:** The authors declare no competing financial interests. **Data and materials availability:** Data analysis MATLAB software routines used to process and generate plots are available on Zenodo (*112*). All data in the main text or the supplementary materials are also available on Zenodo (*112*). All materials are available upon request, which may require a material transfer agreement (MTA). 

## SUPPLEMENTARY MATERIALS

science.org/doi/10.1126/science.adv0134
Figs. S1 to S15
Tables S1 and S2
MDAR Reproducibility Checklist
Movie S1

Submitted 6 December 2024; accepted 16 November 2025
Published online 18 December 2025
10.1126/science.adv0134

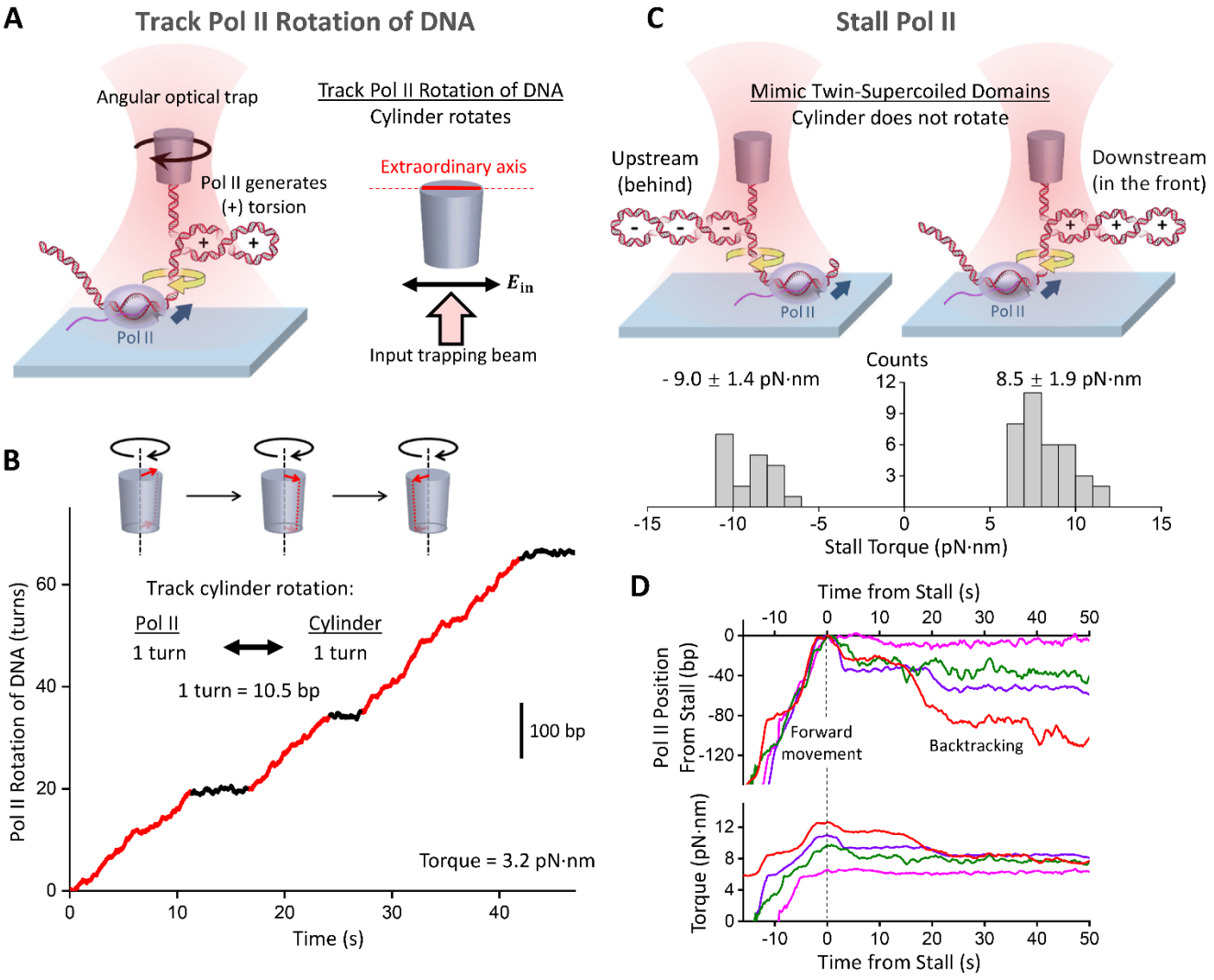


**Fig. 1. Visualizing Pol II rotation and measuring stalling under torsion.** (**A**) An experimental configuration to track Pol II rotation of DNA during transcription using an angular optical trap (AOT). Pol II is torsionally anchored on the surface of a coverslip, and its downstream DNA is torsionally attached to the bottom of a quartz cylinder, which is trapped by the AOT. Pol II elongation generates (+) supercoiling in the downstream DNA. The cylinder rotates to follow Pol II rotation to maintain a constant torque in the DNA. The right panel shows that the extraordinary axis of the cylinder tends to align with the linear polarization of the input trapping beam. The orientation of this axis is accurately detected and informs the angular orientation of the DNA attached to the cylinder. (**B**) A representative real-time trajectory of Pol II rotation of DNA during transcription under a +3.2 pN·nm resistance torque. The scale bar shows the conversion to base pair position of Pol II (approximating nucleotides transcribed). Regions of Pol II steady rotation are marked red, and regions of pausing are marked black. See movie S1 for the corresponding video. (**C**) Pol II stall torque measurements using the AOT. The two cartoons illustrate the experimental configurations to stall Pol II against (−) torsional stress upstream (left) and (+) torsional stress downstream (right), mimicking the "twin-supercoiled-domain" model of transcription. The measured stall torque distributions are shown beneath the corresponding cartoon, with the mean and SD indicated. (**D**) Representative traces of Pol II backtracking upon stalling under (+) torsional stress. Different colors represent different traces. Pol II forward translocates and stalls under increased (+) torque. Upon stalling, Pol II backtracks, as evidenced by the reverse motion.

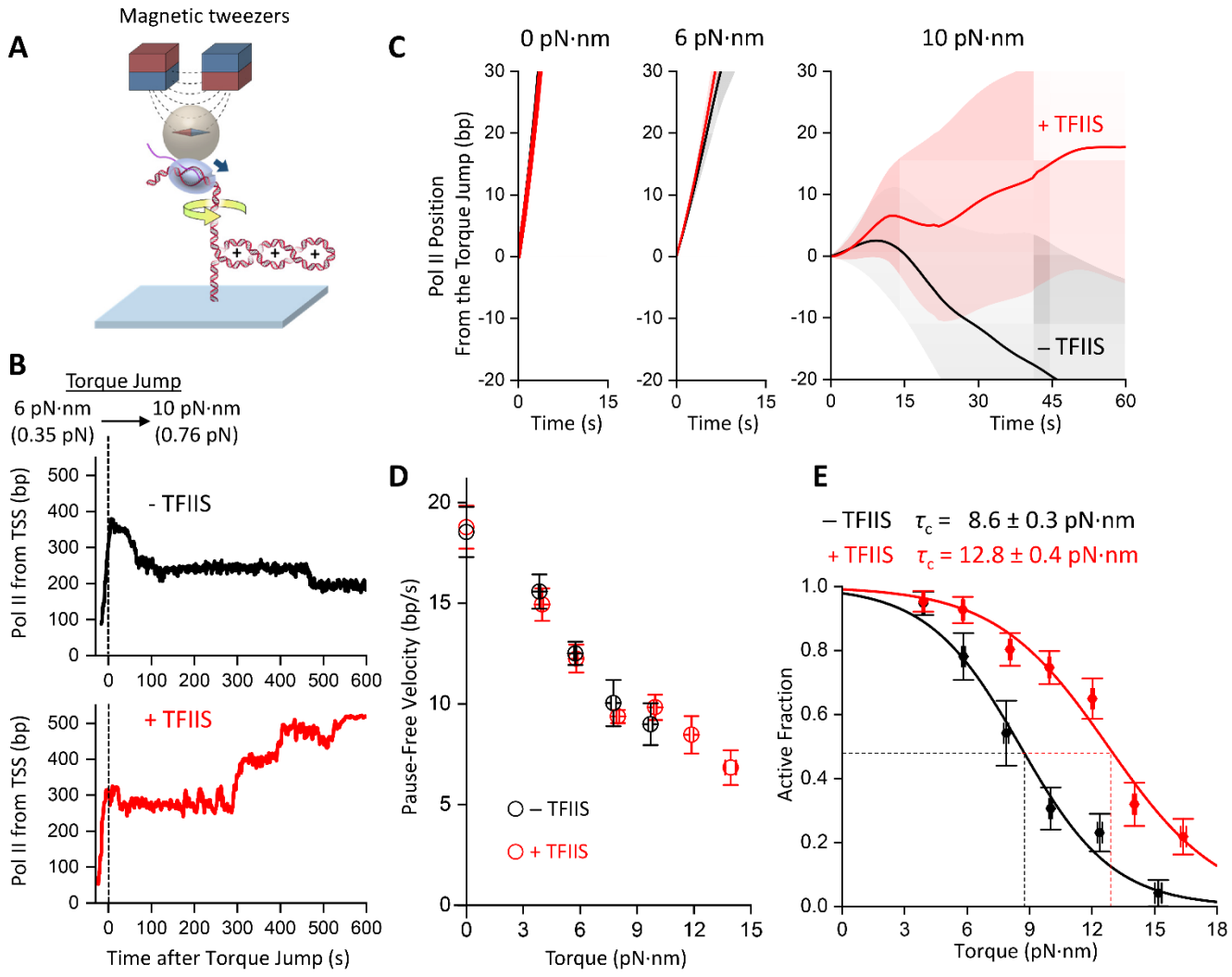


**Fig. 2. TFIIS up-regulates Pol II's ability to transcribe under torsion.** (**A**) Experimental configuration to monitor transcription activity under torsion via magnetic tweezers (MT). Pol II is torsionally anchored to the surface of a magnetic bead, while its downstream DNA is torsionally anchored to the surface of a coverslip. The magnetic bead can be used to manipulate the torsional state of the DNA and the force on the DNA. (**B**) Example traces of Pol II elongation during a torque-jump experiment. In these experiments, NTPs are introduced to the sample chamber before the measurements begin. During the NTP introduction, which typically takes about 20 s, each Pol II molecule may have moved a different distance from the transcription start site (TSS). Since the DNA is buckled during these measurements, the force on the DNA informs the torque in the DNA (fig. S5D). Pol II transcribes under a lower resisting torque, followed by a higher resisting torque. (**C**)The mean trajectory of Pol II elongation under different torques. All traces were aligned at the start of the torque jump ($t$ = 0), with the shaded region for each curve representing 30% of the standard deviation. Without TFIIS: $N$ = 87, 72, and 42 traces for 0, 6, and 10 pN·nm, respectively. With TFIIS: $N$ = 36, 72, and 61 traces for 0, 6, and 10 pN·nm, respectively. (**D**) Torque-velocity relation. Pause-free velocities are shown without and with TFIIS. The error bars represent the SEM, with each data point collected from $N$ = 27-87 traces. (**E**) Active fraction of traces after the torque jump. The active fraction is the fraction of traces remaining active at a given torque. Each curve is fit with a decaying function (Materials and methods) to obtain the critical torque $\tau_c$, at which 50% of traces are active. The fit values and uncertainties without and with TFIIS are also shown.

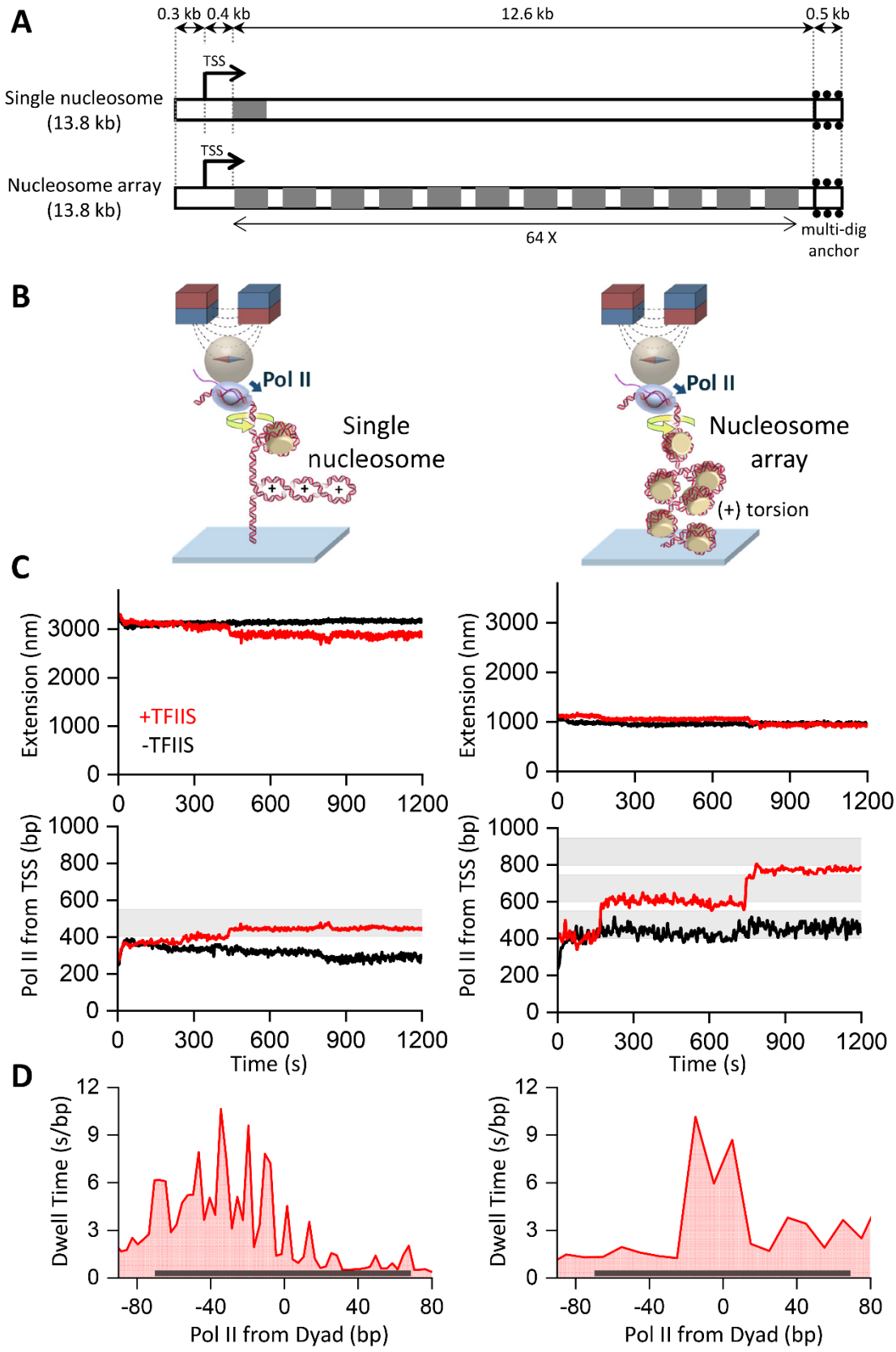

**Fig. 3. A real-time assay of tracking Pol II transcribing through nucleosomes under torsion via magnetic tweezers.** (**A**) The two DNA templates used for transcription through nucleosome experiments (Materials and methods). Both templates have the same total length and the same sequence from the upstream end of the template (−313 bp from TSS) to the exit of the first nucleosome positioning element (NPE) (+550 bp from TSS). Each NPE is indicated as a grey box. The nucleosome array template contains 64 tandem NPE repeats with a repeat length of 197 bp. The 0.5 kb multi-dig anchor at the end of each template is used to tether the template to the coverslip surface. (**B**) Experimental configurations. Pol II is torsionally anchored to the surface of a magnetic bead. The DNA downstream of Pol II contains either a single nucleosome (left) or a nucleosome array (right) and is torsionally anchored to the surface of a coverslip. (**C**) Representative trajectories of Pol II transcribing through nucleosomes under torsion. The left panels show traces from the template containing a single nucleosome. The right panels show traces from the template containing a nucleosome array. The measured extension (top panel) is converted to the Pol II position from the TSS (bottom panel) for each trace (Materials and methods). Each shaded region represents an expected nucleosome position. If a nucleosome dissociates from the DNA, there will be a sudden increase in the DNA extension of about 50 nm, which is not detected during these measurements. (**D**) Pol II dwell time distribution at a nucleosome encounter. The dwell time at each position after Pol II encounters a nucleosome is calculated from Pol II trajectories of $N$ = 58 traces (left panel) and $N$ = 252 traces (right panel) using a "first-passage" method (Materials and methods). The dark grey shaded region indicates the location of the NPE for the first nucleosome encountered.

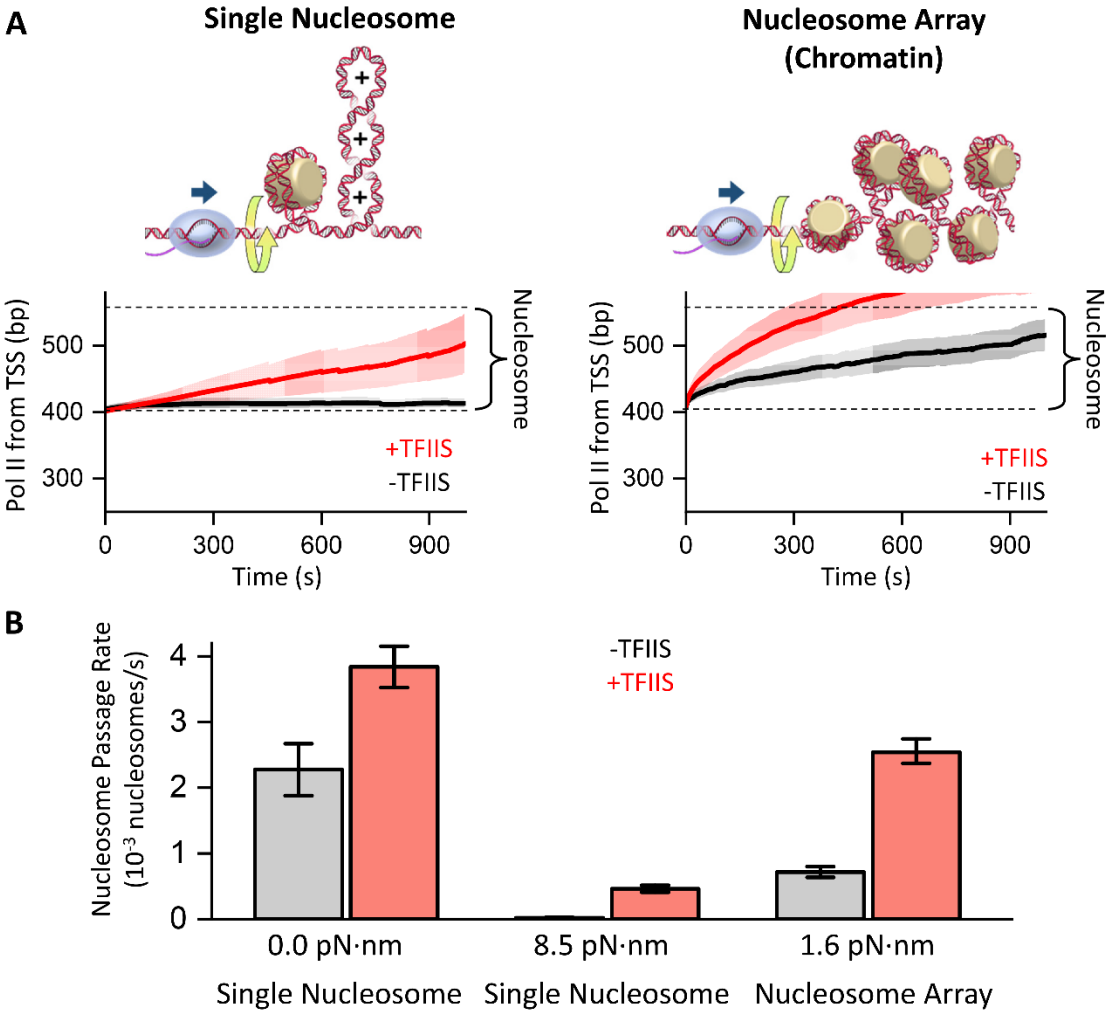


**Fig. 4. Chromatin buffers torsional stress to facilitate transcription.** (**A**) Mean trajectories of Pol II transcription through a nucleosome averaged over many traces. All traces are aligned in time when Pol II reaches the entry of the 1st nucleosome encountered ($t$ = 0), and the "first-passage" method is applied (Materials and methods). The shaded regions represent 30% of the standard deviation. The left panel shows data from the single-nucleosome template (left; $N$ = 86 traces for −TFIIS, $N$ = 215 for +TFIIS). The right panel shows data from the first nucleosome on the chromatin template (right; $N$ = 99 traces for −TFIIS; $N$ = 302 traces for +TFIIS). (**B**) Pol II nucleosome-passage rate. The mean passage rates under torsion were obtained from data shown in A, with the torque value being the torque experienced by Pol II when encountering the nucleosome dyad (Materials and methods). The mean passage rates under zero-torsion of the single-nucleosome template were obtained from data shown in fig. S13. The error bars represent the SEMs.

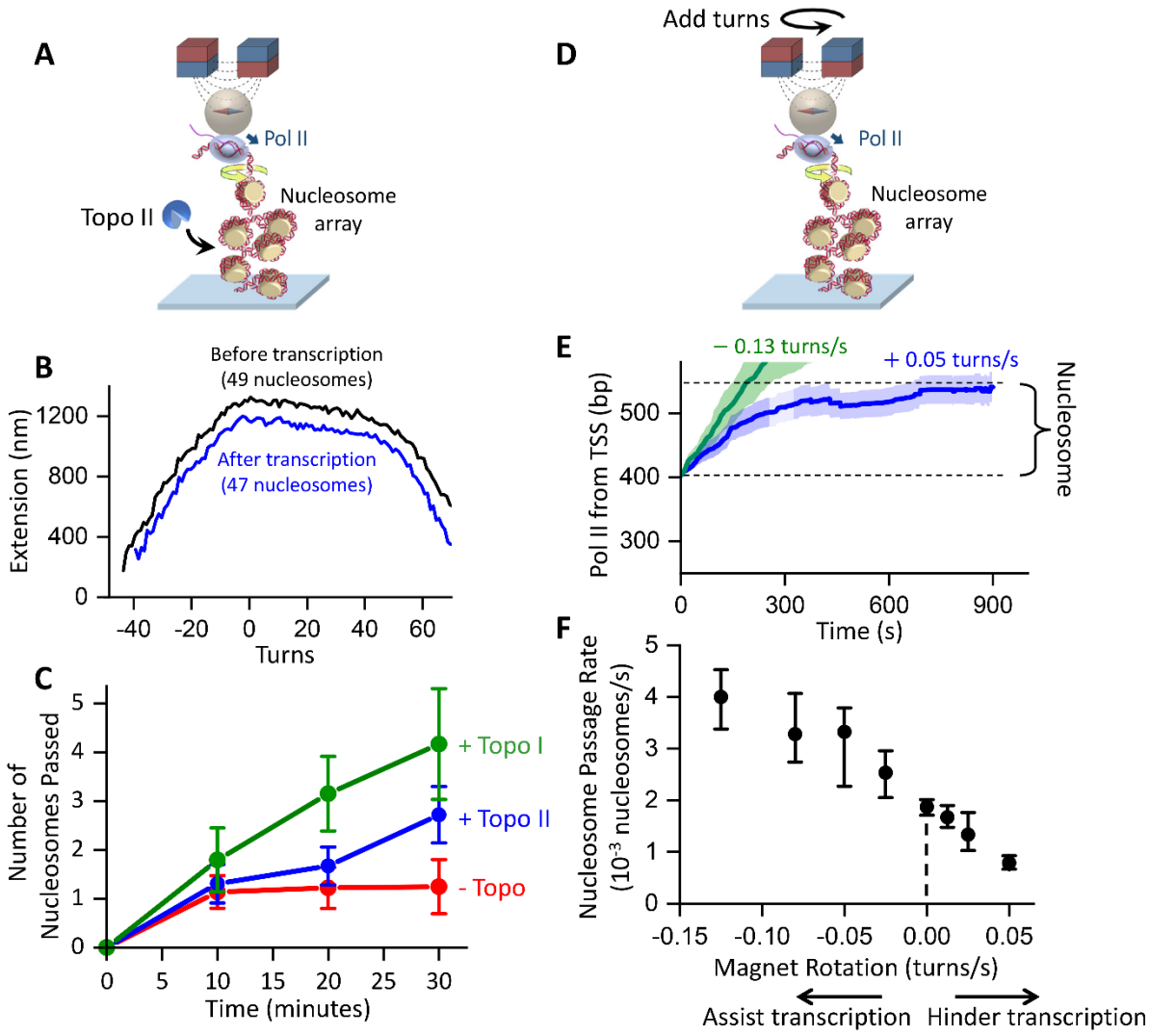


**Fig. 5. Torsional stress modulates nucleosome passage.** (**A**) Experimental configuration of transcription through chromatin in the presence of topo I or II. This configuration is identical to that used in Fig. 3B (right), except for having either topo I or topo II present in the assay. All experiments were carried out in the presence of TFIIS. (**B**) Explanation of the method used to determine the number of nucleosomes passed. The extension-turns relation is determined by the number of nucleosomes and the DNA length between Pol II and the coverslip. Both the width and height of the extension-turns curve decrease after transcription. Shown are example traces where we detect 49 nucleosomes before transcription and 47 nucleosomes after transcription, indicating Pol II having passed 2 nucleosomes during transcription. For clarity of comparison, the curve after transcription is shifted laterally to re-center relative to the curve before transcription. (**C**) The number of nucleosomes passed by Pol II during transcription versus time in the absence of topoisomerases or in the presence of either topo I or topo II. The error bars represent the SEM, with each data point collected from $N$ = 14-33 traces. (**D**) Experimental configuration to modulate torsional stress using the magnetic bead during transcription through chromatin. This configuration is similar to that used in Fig. 3B (right), except that the magnet bead is rotated at a constant rate. All experiments were carried out in the presence of TFIIS. (**E**) Mean trajectories of Pol II transcription through a nucleosome at different magnet rotation rates. All traces were aligned when Pol II reached the entry of the 1st nucleosome encountered ($t$ = 0), with the shaded regions representing 30% of the standard deviation. Shown are examples of magnet rotation rates at +0.05 turns/s (hindering transcription) ($N$ = 30 traces) and −0.13 turns/s (assisting transcription) ($N$ = 49 traces). (**F**) Pol II nucleosome-passage rates at different magnet rotation rates. The mean rates for the passage of the 1st nucleosome encountered are shown, with the error bars representing the ± SEMs, with each data point collected from $N$ = 25-65 traces.